Bioinformatics-Based Identification of Expanded Repeats: A Non-reference Intronic Pentamer Expansion in *RFC1* Causes CANVAS

Haloom Rafehi,[1,2,33] David J. Szmulewicz,[3,4,33] Mark F. Bennett,[1,2,5] Nara L.M. Sobreira,[6] Kate Pope,[7] Katherine R. Smith,[1] Greta Gillies,[7] Peter Diakumis,[8] Egor Dolzhenko,[9] Michael A. Eberle,[9] María García Barcina,[10] David P. Breen,[11,12,13] Andrew M. Chancellor,[14] Phillip D. Cremer,[15,16] Martin B. Delatycki,[7,17] Brent L. Fogel,[18] Anna Hackett,[19,20] G. Michael Halmagyi,[21,22] Solange Kapetanovic,[23] Anthony Lang,[24,25] Stuart Mossman,[26] Weiyi Mu,[6] Peter Patrikios,[27] Susan L. Perlman,[28] Ian Rosemergy,[29] Elsdon Storey,[30] Shaun R.D. Watson,[31] Michael A. Wilson,[7] David S. Zee,[32] David Valle,[6] David J. Amor,[7,17] Melanie Bahlo,[1,2,34] and Paul J. Lockhart[7,17,34,*]

Genomic technologies such as next-generation sequencing (NGS) are revolutionizing molecular diagnostics and clinical medicine. However, these approaches have proven inefficient at identifying pathogenic repeat expansions. Here, we apply a collection of bioinformatics tools that can be utilized to identify either known or novel expanded repeat sequences in NGS data. We performed genetic studies of a cohort of 35 individuals from 22 families with a clinical diagnosis of cerebellar ataxia with neuropathy and bilateral vestibular areflexia syndrome (CANVAS). Analysis of whole-genome sequence (WGS) data with five independent algorithms identified a recessively inherited intronic repeat expansion [$(AAGGG)_{exp}$] in the gene encoding Replication Factor C1 (*RFC1*). This motif, not reported in the reference sequence, localized to an Alu element and replaced the reference $(AAAAG)_{11}$ short tandem repeat. Genetic analyses confirmed the pathogenic expansion in 18 of 22 CANVAS-affected families and identified a core ancestral haplotype, estimated to have arisen in Europe more than twenty-five thousand years ago. WGS of the four *RFC1*-negative CANVAS-affected families identified plausible variants in three, with genomic re-diagnosis of SCA3, spastic ataxia of the Charlevoix-Saguenay type, and SCA45. This study identified the genetic basis of CANVAS and demonstrated that these improved bioinformatics tools increase the diagnostic utility of WGS to determine the genetic basis of a heterogeneous group of clinically overlapping neurogenetic disorders.

Introduction

Repetitive DNA sequences constitute approximately one third of the genome and are thought to contribute to diversity within and between species.[1] Microsatellites or short tandem repeats (STRs) are mini-repeats of DNA, typically two to five base-pairs in length, which are usually present in a concatamer of between 5 and 50 repeated elements. There are thousands of STRs scattered through the human genome and recent studies have suggested important roles for STRs in the regulation of gene expression.[2,3] STRs display considerable variability in length between individuals, which is presumed to have no detrimental consequences for humans[4,5] unless the repeat number is expanded beyond a gene-specific threshold.[6,7] Pathogenic repeat expansions (REs) have been shown to underlie at

[1]Population Health and Immunity Division, The Walter and Eliza Hall Institute of Medical Research, 1G Royal Parade, Parkville, VIC 3052, Australia; [2]Department of Medical Biology, University of Melbourne, 1G Royal Parade, Parkville, VIC 3052, Australia; [3]Cerebellar Ataxia Clinic, Neuroscience Department, Alfred Health, Melbourne, VIC 3004, Australia; [4]Balance Disorders and Ataxia Service, Royal Victorian Eye & Ear Hospital, East Melbourne, VIC 3002, Australia; [5]Epilepsy Research Centre, Department of Medicine, University of Melbourne, Austin Health, 245 Burgundy Street, Heidelberg, VIC 3084, Australia; [6]McKusick-Nathans Institute of Genetic Medicine, Johns Hopkins University School of Medicine, Baltimore, MD 21205, USA; [7]Bruce Lefroy Centre, Murdoch Children's Research Institute, Flemington Rd, Parkville, VIC 3052, Australia; [8]University of Melbourne Centre for Cancer Research, Victorian Comprehensive Cancer Centre, 305 Grattan Street, Melbourne, VIC 3000, Australia; [9]Illumina Inc, 5200 Illumina Way, San Diego, CA 92122, USA; [10]Genetic Unit, Basurto University Hospital, OSI Bilbao-Basurto, avenida Montevideo 18, 48013 Bilbao, Spain; [11]Centre for Clinical Brain Sciences, University of Edinburgh, Edinburgh EH16 4SB, Scotland; [12]Anne Rowling Regenerative Neurology Clinic, University of Edinburgh, Edinburgh EH16 4SB, Scotland; [13]Usher Institute of Population Health Sciences and Informatics, University of Edinburgh, Edinburgh EH16 4UX, Scotland; [14]Department of Neurology, Tauranga Hospital, Private Bag, Cameron Road, Tauranga 3171, New Zealand; [15]University of Sydney, Camperdown, NSW 2006, Australia; [16]Royal North Shore Hospital, Pacific Hwy, St Leonards, NSW 2065, Australia; [17]Department of Paediatrics, University of Melbourne, Royal Children's Hospital, Flemington Rd, Parkville, VIC 3052, Australia; [18]Departments of Neurology and Human Genetics, David Geffen School of Medicine, University of California, Los Angeles, CA 90095, USA; [19]Hunter Genetics, Hunter New England Health Service, Waratah, Newcastle, NSW 2300, Australia; [20]University of Newcastle, Newcastle, NSW 2300, Australia; [21]Neurology Department, Royal Prince Alfred Hospital, Camperdown, NSW 2050, Australia; [22]Central Clinical School, University of Sydney, Camperdown, NSW 2050, Australia; [23]Servicio de Neurología, Hospital de Basurto, Avenida de Montevideo 18, 48013 Bilbao, Bizkaia, Spain; [24]Edmond J. Safra Program in Parkinson disease and the Morton and Gloria Shulman Movement Disorders Clinic, Toronto Western Hospital, Toronto, ON M5T 2S8, Canada; [25]Department of Medicine, Division of Neurology, University Health Network and the University of Toronto, Toronto, ON M5T 2S8, Canada; [26]Department of Neurology, Wellington Hospital, Wellington 6021, New Zealand; [27]Sunshine Neurology, Maroochydore, QLD 4558, Australia; [28]Department of Neurology, David Geffen School of Medicine, University of California, Los Angeles, CA 90095, USA; [29]Department of Neurology, Wellington Hospital, Newtown, Wellington 6021, New Zealand; [30]Department of Neuroscience, Central Clinical School, Monash University, Alfred Hospital Campus, Commercial Road, Melbourne, VIC 3004, Australia; [31]Institute of Neurological Sciences, Prince of Wales Hospital, Randwick, NSW 2031, Australia; [32]Department of Neurology, Johns Hopkins Hospital, Baltimore, MD 21287, USA
[33]These authors contributed equally to this work
[34]These authors contributed equally to this work
*Correspondence: paul.lockhart@mcri.edu.au
https://doi.org/10.1016/j.ajhg.2019.05.016.

least 30 inherited human diseases, the majority being disorders of the nervous system.[8] These disorders, which variably have autosomal-dominant, autosomal-recessive, and X-linked inheritance, have an overall prevalence of ~1:20,000.[9] They display a broad onset age and are characterized by progressive cerebellar ataxia with dysarthria, oculomotor abnormalities, cognitive dysfunction, and other symptoms (see GeneReviews in Web Resources). Additional novel pathogenic REs likely remain to be identified. For example, putative spinocerebellar ataxia (SCA) loci, including SCA25 (MIM: 608703) and SCA30 (MIM: 613371), remain to be identified, and unsolved hereditary ataxias such as cerebellar ataxia with neuropathy and bilateral vestibular areflexia syndrome (CANVAS [MIM: 614575]) display extensive clinical similarities with known RE disorders.

CANVAS is a cerebellar ataxia with combined cerebellar, vestibular, and somatosensory dysfunction.[11,12] Historically, individuals with CANVAS have been assigned the diagnosis of idiopathic late-onset cerebellar ataxia.[13] More recently, CANVAS is clinically recognized and has been incorporated into the contemporary research and teaching of both cerebellar and vestibular diseases.[14,15] Unifying the oto- and neuropathology, CANVAS is a neuronopathy (ganglionopathy) affecting the vestibular[16] and dorsal root ganglia.[17] The progression of these clinical features can be measured longitudinally using a specific neurophysiological protocol.[18] A characteristic radiological pattern of cerebellar atrophy has also been described and verified on post-mortem pathology.[11] The characteristic oculomotor abnormality seen in combined cerebellar and vestibular impairment is the visually enhanced vestibulo-ocular reflex (VVOR), and this can now be evaluated using a commercially available instrumented assessment tool.[19–21] Altogether, these advances have allowed the formulation of diagnostic criteria to aid identification of CANVAS, contributing both research and clinical benefits including improved prognostication and targeted management.[12,14] While detailed clinical findings have driven gene discovery in RE disorders such as Friedreich ataxia,[22] the underlying genetic cause(s) of CANVAS has, until very recently, remained elusive (see below).

The majority of individuals and families with CANVAS have been identified in individuals of European ancestry, although CANVAS has recently been reported in two individuals of Japanese ethnicity, a 68-year-old male[23] and a 76-year-old female.[24] A genetic cause of CANVAS is highly plausible given the observation of 13 affected siblings and families with multiple affected individuals over several generations.[12] The pattern of inheritance suggests an autosomal-recessive trait, although autosomal-dominant inheritance with incomplete penetrance cannot be excluded. CANVAS symptoms overlap considerably with SCA3 (also known as Machado-Joseph disease [MIM: 109150]) and Friedreich ataxia (MIM: 229300), both genetic forms of ataxia caused by the inheritance of a pathogenic RE. These observations are consistent with the hypothesis that a novel pathogenic STR expansion may underlie CANVAS.

Historically, the detection of REs has been time consuming and expensive. Indeed, it is only in recent years that computational methods have been developed to screen for RE in short-read whole-exome sequence (WES) and WGS data,[25] leading to the discovery of previously undescribed, disease-causing REs. For example, a pentanucleotide RE was identified to underlie autosomal-dominant spinocerebellar ataxia 37 (SCA37 [MIM: 615945]).[26] Moreover, pathogenic REs of intronic pentamers $(TTTCA)_n$ and $(TTTTA)_n$ were identified as the cause of benign adult familial myoclonus epilepsy locus 1, 6, and 7 (BAFME1 [MIM: 618073], BAFME6 [MIM: 618074], BAFME1 [MIM: 618075]).[27]

A number of bioinformatics tools now exist that allow screening of short-read sequencing data for expanded STRs.[25] Initially, STR detection tools, such as lobSTR and hipSTR, were limited to short STRs that were encompassed by a single sequencing read. However, in the last two years, multiple methods have been released that can screen WES and WGS datasets for REs without being limited by read length. These include ExpansionHunter (EH),[28] exSTRa,[8] TREDPARSE,[29] STRetch,[30] and GangSTR.[31] These are all reference based methods, i.e., they rely on a catalog of STR loci and motifs and are therefore limited to detecting expansion of previously defined STRs, such as those cataloged in the UCSC track. Moreover, the normal variability in STR length and repeat composition remains poorly described, particularly for rare STRs or those larger than ~100 bp. Therefore, there is a need for bioinformatics tools that are unbiased to the limited catalogs of STR loci available. Ideally, these tools will be able to search genome-wide for expanded repeat sequences in NGS data, independent of prior knowledge of either the location or composition of the RE. Here, we utilized a STR reference-free method called Expansion Hunter *De Novo* (EHdn), in combination with multiple reference-based tools, to show that CANVAS is caused by the homozygous inheritance of a previously undescribed expanded intronic pentamer $[(AAGGG)_{exp}]$ in the gene encoding Replication Factor C Subunit 1 (*RFC1*). An independent study, published while this work was under review, similarly identified this causal pentamer in *RFC1*. Cortese and colleagues defined a small linkage region from ten families with CANVAS and the causative RE was identified by WGS and visual inspection of the aligned read pairs inside the linkage region.[32]

Material and Methods

Recruitment, Linkage, and Next-Generation Sequence Data

The Royal Children's Hospital Human Research Ethics Committee approved the study (HREC 28097). Informed consent was obtained from all participants and clinical details were collected from clinical assessments and review of medical records. Genomic DNA was isolated from peripheral blood. Single-nucleotide polymorphism (SNP) genotype data were generated for two affected

siblings from three families (CANVAS1, 2, and 3) and all six siblings from family CANVAS4 using the Illumina Infinium HumanOmniExpress BeadChip genotyping array. SNP genotypes for individuals from CANVAS9 were extracted from WES data.[33] Parametric multipoint linkage analysis was subsequently performed using LINKDATAGEN and MERLIN[34,35] specifying a rare recessive disease model with complete penetrance, and overlapping linkage signals were detected using BEDtools.[36] WES was performed on individuals from CANVAS9 using Agilent SureSelect XT Human All exon V5 + UTR on the Illumina HiSeq2000 platform at 50× mean coverage. WES was performed on an additional 23 individuals from 15 families in collaboration with the Johns Hopkins Center for Inherited Disease Research (CIDR) as part of the Baylor-Hopkins Center for Mendelian Genomics (BHCMG). WGS was performed in two stages. Libraries for the first round of samples, including two affected individuals from CANVAS1 and CANVAS9 and 31 individuals lacking a clinical diagnosis of CANVAS (subsequently referred to as control subjects although some have a diagnosis other than CANVAS), were prepared using the TruSeq nano PCR-based Library Preparation Kit and sequenced on the Illumina HiSeq X platform. Libraries for the second round of WGS, including affected individuals with evidence of an alternate RE motif (CANVAS2 and 8) or lacking the pathogenic RE in *RFC1* (CANVAS11, 13, 17, and 19), were prepared using the TruSeq PCR-free DNA HT Library Preparation Kit and sequenced on the Illumina NovaSeq 6000 platform. PCR-free WGS data from 69 unrelated Coriell control subjects[28] was obtained from Illumina. GTEx samples (SRA files, 133 WGS with matching cerebellar RNA-seq) were downloaded from the dbGAP (phs000424.v7.p2).

Alignment and Variant Calling

Alignment and haplotype calling were performed based on the GATK best practice pipeline. All WES and WGS datasets were aligned to the hg19 reference genome using BWA-mem, then duplicate marking, local realignment, and recalibration were performed with GATK. Merged VCF files were annotated using vcfanno[37] and ANNOVAR.[38] Candidate variant filtering was performed using CAVALIER, an R package for variant interpretation in NGS data (Web Resources). Standard variant calling was performed on WGS data for CANVAS samples negative for the pathogenic RE in *RFC1*. Candidate variants were defined as (1) occurring in known ataxia genes, as defined by OMIM, (2) exonic, with a minor allele frequency of less than 0.0001 in gnomAD (both genome and exome data), and (3) predicted pathogenic by both SIFT and PolyPhen2. RNA-seq data was aligned to the hg19 reference genome (ENSEMBL Homo_sapiens.GRCh37.75) using STAR.[39] Reads were summarized by gene ID into a counts matrix using featureCounts[40] (quality score $\geq$ 10) and converted to log10 of the counts per million using limma.[41]

STR Analysis

Genome-wide screening for putative REs was performed using Expansion Hunter Denovo (EHdn) v.0.6.2, an open-source method that is being developed by Illumina, the Walter Eliza Hall Institute, and others. EHdn operates by performing a genome-wide search for read pairs where one mate has confident alignment (anchor) and the second mate consists of repetition of a repeat motif (in-repeat read). The program reports the counts of in-repeat reads with anchor mates stratified by the repeat motif and genomic position of their anchor mate. For this analysis we defined a confidently aligned read as one aligned with MAPQ of 50 or above. The counts of in-repeat reads with anchor mates were subsequently compared for each region in case subjects (CANVAS) and control subjects using a permutation test (10^6 permutations). The resulting p values were used to rank candidate sites with higher counts in individuals with CANVAS than in the control subjects for further computational validation. These candidates were subsequently annotated with ANNOVAR.

Computational validation was performed using five independent STR detection tools for short-read NGS after updating the STR catalog reference files to incorporate the identified motifs. The RE candidates were screened in the two individuals with CANVAS and the 31 non-CANVAS control subjects using exSTRa and EH, then the top candidate [$(AAGGG)_{exp}$ STR in *RFC1*] was further validated with TREDPARSE, GangSTR, and STRetch. All tools were used with default parameters, with the following additional parameters for EH: read-depth of 30 and min-anchor-mapq of 20. All five tools were also used to screen for the $(AAGGG)_{exp}$ *RFC1* STR in the 69 Coriell control WGS datasets. A short-list of $(AAGGG)_{exp}$ carriers was generated based on consensus calling from at least four of the five tools.

Individuals diagnosed with CANVAS lacking the $(AAGGG)_{exp}$ *RFC1* RE were further screened with EHdn for novel STRs and for known pathogenic STRs using exSTRa and EH. The WES datasets could not be analyzed for the $(AAGGG)_{exp}$ *RFC1* RE as the intronic locus (chr4:39350045–39350095, hg19) was not captured during library preparation. However, the region was visualized in the alignment using the Integrative Genomics Viewer (IGV) to identify potential off-target reads, which could provide supportive evidence for the presence of the $(AAGGG)_{exp}$ motif. Only samples with at least one read mapping at the STR in the *RFC1* locus were considered.

Haplotyping and Mutation Dating

Haplotyping was performed on the WES data. Variants were filtered based on read depth ($\geq$30), including both exonic and non-exonic variants. A core haplotype was defined based on sharing among a majority of affected individuals. A method based on haplotype sharing[42] was used to determine the most recent common ancestor (MRCA) from whom the core haplotype was inherited, as well as dating additional sub-haplotypes shared by clusters of individuals, which are likely to be individuals with a MRCA who is more recent than that for the whole group (see Mutation dating in Web Resources).

Molecular Genetic Studies

We designed a PCR assay to test for presence of additional inserted sequence, not present in the reference database, at the *RFC1* STR. The primers (Table S1) flank the STR and are predicted to amplify a 253 bp fragment using standard PCR conditions with a 30 s extension cycle. Presence of the pathogenic *RFC1* RE was tested by repeat-primed PCR utilizing three primers: TPP_CANVAS_FAM_2F, 5R_TPP_M13R_CANVAS_RE_R, and TPP_M13R (Table S1). The FAM labeled forward primer is locus specific, while the repeat-specific primer (5R_TPP) includes a tag M13R sequence. PCR was performed in a 20 μL reaction with 20 ng genomic DNA, 0.8 μM of both the FAM labeled forward primer and TPP_M13R, and 0.2 μM 5R_TPP using GoTaq Long PCR Polymerase (Promega). A standard 60TD55 protocol was utilized (94°C denaturation for 30 s, 60TD55°C anneal for 30 s, and 72°C extension for 2 min), products were detected on an ABI3730xl DNA Analyzer and visualized using PeakScanner 2 (Applied Biosystems).

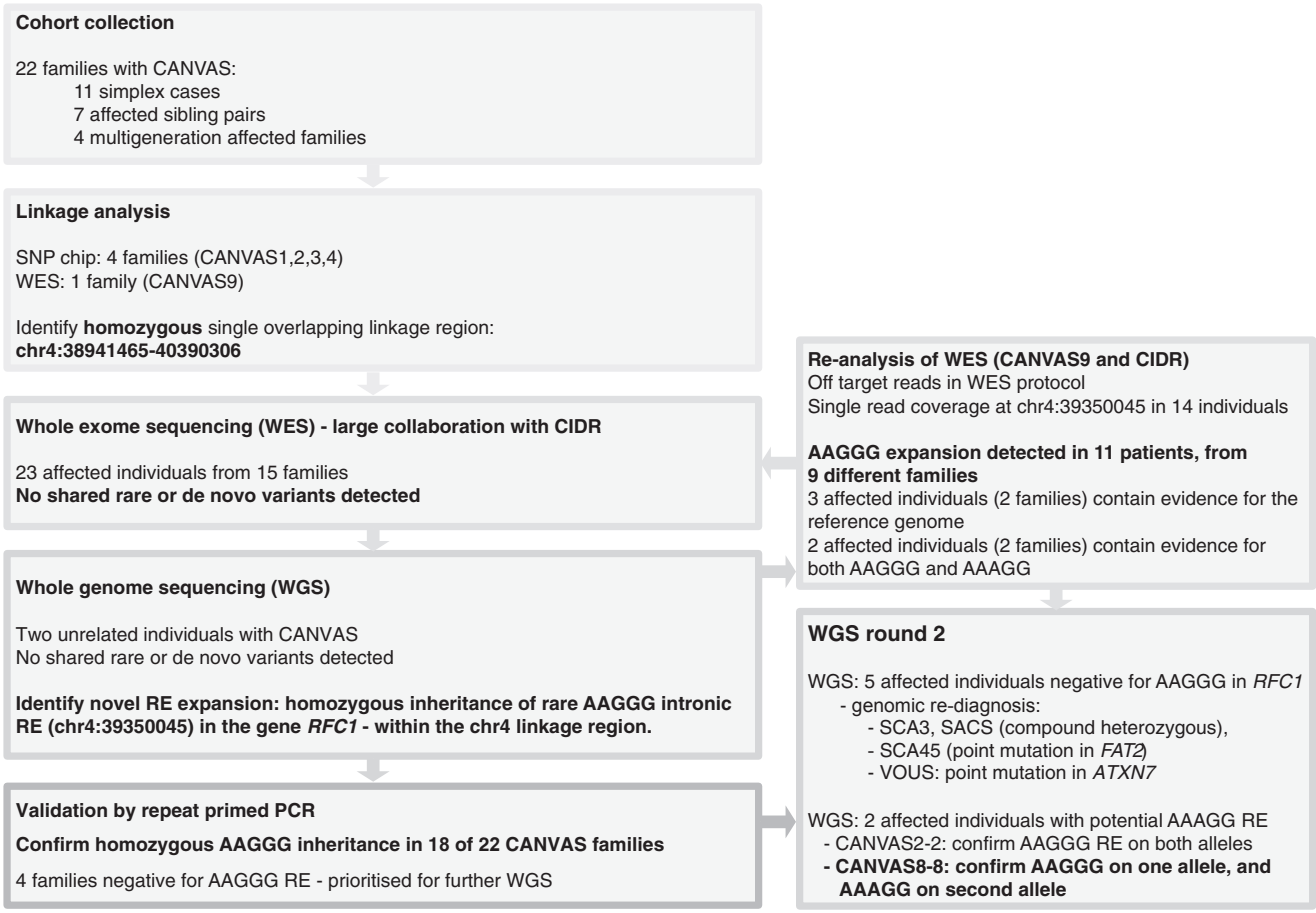

Figure 1. Overview of the CANVAS Study and Genetic Investigations Performed

Results

Case Recruitment

The workflow for this study is summarized in Figure 1. Individuals with a clinical diagnosis of CANVAS were recruited following neurological assessment and investigation in accordance with published guidelines.[43] While variable between case subjects, data leading to the clinical diagnosis included evidence of combined cerebellar and bilateral vestibular impairment, cerebellar atrophy on MRI, neurophysiological evidence of impaired sensory nerve function, and negative genetic testing for pathogenic RE at common SCA loci (typically *SCA1*, *2*, *3*, *6*, and *7*) and *FRDA* (Friedreich ataxia, FRDA). In total, the cohort consisted of 35 individuals with a clinical diagnosis of CANVAS (Table 1). The individuals came from 11 families with a single affected individual, 7 families with affected sib pairs and 4 larger/multigenerational families (Figure S1). A full clinical description of the cohort will be reported in a forthcoming manuscript.

Linkage Analysis

CANVAS typically presents in families with one or multiple affected individuals in a single generation, consistent with a recessive inheritance. For example, in the second-degree consanguineous family CANVAS9, four siblings were diagnosed with CANVAS and two were classified as unaffected at the time phenotyping was performed (Figure 2A). Parametric multipoint linkage analysis was performed on five CANVAS-affected families (CANVAS1, 2, 3, 4, and 9; Figure S1) specifying a rare recessive disease model with complete penetrance. This identified linkage regions with logarithm of odds (LOD) scores ranging from 0.6 for smaller pedigrees (two affected siblings) to a statistically significant linkage region on chromosome 4 in CANVAS9 (LOD = 3.25, Figure 2B). Intersection of the linkage regions from the five families identified a single region on chromosome four (chr4:38887351–40463592, hg19, combined LOD = 7.04) common to all families (Figure 2C). CNV analysis utilizing PennCNV did not identify any potential copy number variants in the minimal linkage region.[44] The 1.5 Mb shared region contains 42 genes, of which 14 are protein coding, none with any association with ataxia in OMIM or the published literature (Table S2).

Large-Scale WES Analysis Did Not Identify Candidate Pathogenic Variants

WES was used to screen 27 affected individuals with CANVAS from 15 families for potentially pathogenic rare variants (MAF < 0.001) shared across multiple pedigrees

Table 1. Clinical Features and Genetic Analysis of *RFC1* Locus in Study Participants

Family	Participants (Sex)	SNP Array	WES	WGS	*RFC1* STR in WES	PCR Wild-Type Allele	Repeat-Primed PCR	Genetic Diagnosis	Haplotype	Ethnicity
CANVAS1	2 (F)	Y	Y	Y	ND	N	Y	CANVAS	A/other	European
CANVAS2	2 (M)	Y	Y	Y	AAGGG and AAAGG	N	Y	CANVAS	A	European
CANVAS3	2 (F)	Y	Y	N	AAGGG	N	Y	CANVAS	A	European
CANVAS4	4 (3M,1F)	Y	Y	N	AAGGG	N	Y	CANVAS	A	Greek-Cypriot
CANVAS5	2 (M,F)	N	N	N	ND	N	Y	CANVAS	not assessed	not reported
CANVAS6	2 (M)	N	Y	N	AAGGG	N	Y	CANVAS	A	Lithuanian/Latvian
CANVAS7	1 (M)	N	Y	N	ND	N	Y	CANVAS	A	European-Maori
CANVAS8	1 (F)	N	Y	Y	AAGGG and AAAGG	N	Y	CANVAS	A/other	European
CANVAS9	4 (1M,3F)	N	Y	Y	AAGGG	N	Y	CANVAS	A	Lebanese
CANVAS10	1 (M)	N	Y	N	AAGGG	N	Y	CANVAS	A	European
CANVAS11	1 (M)	N	Y	Y	ND	Y	N	?	NA	Anglo-saxon
CANVAS12	1 (M)	N	Y	N	ND	N	Y	CANVAS	A	Turkish
CANVAS13	1 (M)	N	Y	Y	reference	Y	N	SCA3	NA	Martinique
CANVAS14	1 (M)	N	Y	N	AAGGG	N	Y	CANVAS	other*	European
CANVAS16	1 (F)	N	N	N	NA	N	Y	CANVAS	not assessed	European
CANVAS17	2 (M)	N	Y	Y	reference	Y	N	SACS	NA	European
CANVAS18	1 (F)	N	Y	N	ND	N	Y	CANVAS	A	European-Maori
CANVAS19	1 (F)	N	N	Y	NA	Y	N	SCA45	not assessed	European
CANVAS20	2 (1M,1F)	N	N	N	NA	N	Y	CANVAS	not assessed	Spanish
CANVAS21	1 (M)	N	N	N	NA	N	Y	CANVAS	not assessed	Indian
CANVAS22	1 (M)	N	N	N	NA	N	Y	CANVAS	not assessed	Hungarian
CANVAS23	1 (U)	N	N	N	NA	N	Y	CANVAS	not assessed	not reported

Abbreviations: M, male; F, female; U, deidentified; NA, not applicable; ND, not detected; Other*, a different haplotype OR shortened A haplotpye. The gene reference sequences utilized were GenBank: NC_000004.11 and NM_002913.4 (RFC1).

in a homozygous or compound heterozygous inheritance pattern. No candidate mutations were detected, either within the chromosome 4 linkage region or elsewhere in the genome.

Identification of an Undescribed $(AAGGG)_{exp}$ RE in the Linkage Region

The lack of candidate variants identified from the WES data suggested the possibility of (1) intronic or intergenic mutations or (2) that CANVAS might be caused by a non-standard mutation, such as a pathogenic RE of an STR. Therefore, WGS was performed on two individuals from different pedigrees (CANVAS1 and 9) who share the chr4 linkage region. EHdn was used to perform a genome-wide screen for STRs in the two individuals with CANVAS compared to WGS data from 31 unrelated control subjects. This identified 19 regions with a p value < 0.005 (Table S3), although genome-wide significance could not be achieved after adjustment for multiple testing due to the skewed ratio of the number of case subjects to control subjects (2 versus 31). These candidate STRs were visualized with the Integrative Genomics Viewer (IGV) tool, which suggested that the $(AAGGG)_{exp}$ STR within intron 2 of the gene encoding Replication Factor C1 (*RFC1*) was likely real and present in both alleles in the affected individuals, consistent with the recessive inheritance pattern hypothesized for CANVAS (Figure S2). In addition, this was the only candidate that (1) was localized to the chr4 linkage region and (2) was able to be validated using existing STR detection tools (see below). In both individuals with CANVAS, the $(AAGGG)_{exp}$ pentamer replaced an $(AAAAG)_{11}$ motif located at the same position in the reference genome (chr4:39350045–39350095, hg19) and appeared to be significantly expanded compared to controls. Visualization of the region in the UCSC genome browser identified that the reference motif $(AAAAG)_{11}$ is the 3′ end of an Alu element, AluSx3. In individuals with CANVAS, the $(AAAAG)_{11}$ motif is substituted by the $(AAGGG)_{exp}$ motif, with potential interruptions to the Alu element (Figure 2D).

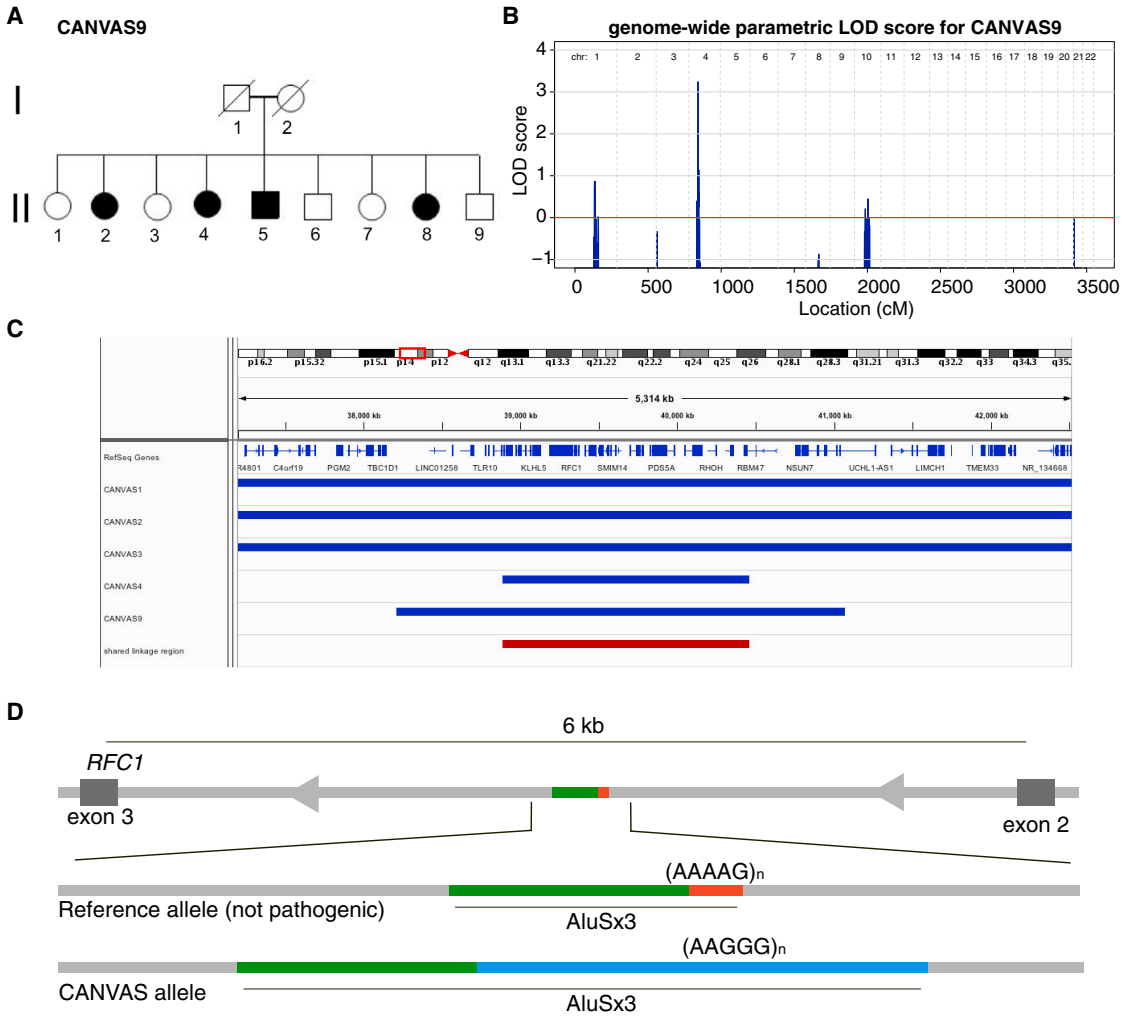

Figure 2. Linkage of the CANVAS Locus to Chromosome 4 and Identification of $(AAGGG)_{exp}$ Intronic Insertion in *RFC1*
(A) The pedigree of the family CANVAS9 highlights the apparent recessive inheritance pattern.
(B) Linkage analysis of CANVAS9 identified significant linkage to chromosome 4 (LOD = 3.25).
(C) Linkage regions for individual families CANVAS1, 2, 3, 4, and 9 are shown in blue and the overlapping region shown in red (chr4:38887351–40463592, combined LOD = 7.04).
(D) STR analysis of WGS from two unrelated individuals with CANVAS identified an expanded STR in the second intron of *RFC1*. The $(AAAAG)_{11}$ motif that is present in the reference genome and part of an existing Alu element (AluSx3) is replaced by the $(AAGGG)_{exp}$ RE.

Confirmation of $(AAGGG)_{exp}$ STR in Off-Target WES Reads

While WGS was only performed in two individuals with CANVAS, the majority of the cohort (n = 27) was analyzed by WES. The putative pathogenic CANVAS RE is located in intron 2 of *RFC1*, 2,863 bp downstream of exon 2 and 2,952 bp upstream of exon 3. Therefore WES data are *a priori* assumed to be uninformative for this RE as it is not targeted during DNA capture. However, given that WES data includes off-target reads, we hypothesized that some reads might map to the *RFC1* RE locus. Visual assessment of the WES data in IGV identified 14 individuals with informative reads; the maximum off-target read coverage at this locus was two, with a median of one read. While 3 individuals only had reads that correspond to the reference genome STR sequence (AAAAG), 11 affected individuals from 9 families had reads containing (AAGGG) repeats (Table 1). Furthermore, single affected individuals from families CANVAS2 and CANVAS8 had single, independent reads identifying (AAGGG) and (AAAGG) motifs at the *RFC1* STR locus. This observation raised the possibility that CANVAS might result from pathogenic expansions of different pentanucleotide motifs.

Computational Validation with Existing STR Detection Tools

Multiple tools have been developed in recent years that test for the presence of REs at pre-defined STRs. Therefore, we inserted the *RFC1* STR motifs into the STR reference files and used exSTRa, EH, TREDPARSE, STRetch, and GangSTR to estimate the size of the STR and/or detect REs in the WGS data from the two original CANVAS samples (CANVAS1 and 9) and seven additional individuals with CANVAS. The seven additional CANVAS samples selected for WGS were those with WES evidence for an alternate

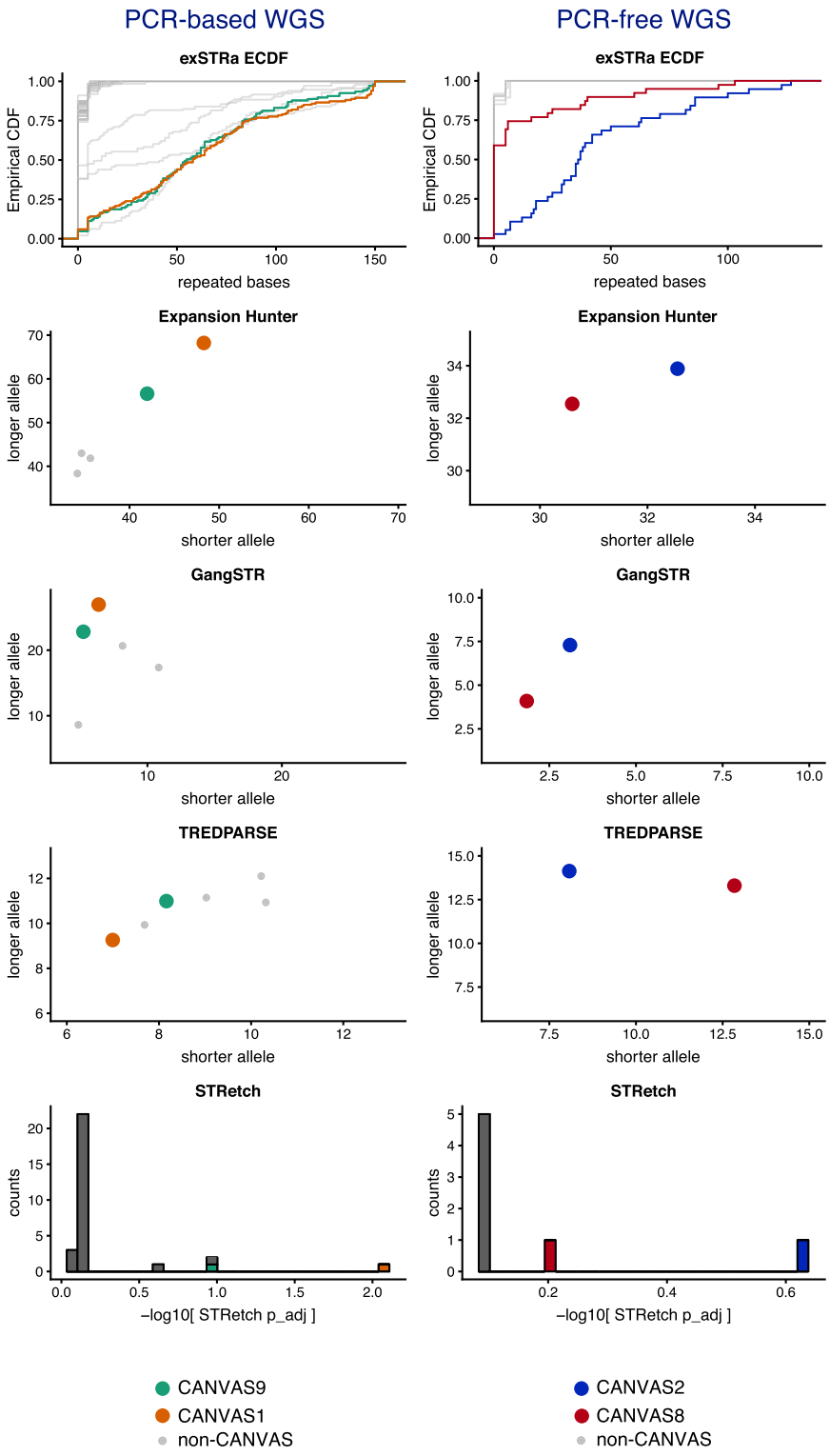

Figure 3. Computational Validation of the $(AAGGG)_{exp}$ RE

The $(AAGGG)_{exp}$ RE at the coordinates chr4:39350045–39350095 was added to the reference databases of the tools exSTRa, EH, GangSTR, TREDPARSE, and STRetch and WGS data from four unrelated individuals with CANVAS was analyzed (CANVAS1, orange; CANVAS2, blue; CANVAS8, red; and CANVAS9, green). The non-CANVAS control subjects are presented in gray. Plots have been divided into PCR-based and PCR-free WGS (left and right columns, respectively). The Y and X axes for ExpansionHunter, GangSTR, and TREDPARSE refer to the number of repeat units on the longer and shorter allele per individual, respectively. The y axis for the STRetch plot refers to the number of individuals.

(AAAGG) motif (families CANVAS2 and 8), and those who did not appear to have a RE at the *RFC1* locus based on the PCR/RP-PCR studies described below (CANVAS11, 13, 17, and 19 families). The library preparation this second round of WGS was PCR free as PCR amplification has previously been shown to affect RE detection.[8] Using exSTRa, we confirmed the homozygous inheritance of the $(AAGGG)_{exp}$ RE in three individuals (CANVAS1, 2, and 9; Figure 3). The empirical cumulative distribution function (ECDF) pattern for CANVAS2 is consistent with the presence of one shorter and one longer $(AAGGG)_{exp}$ RE, while CANVAS8 appears to only have a single $(AAGGG)_{exp}$ allele. Screening of all datasets for the $(AAAGG)_{exp}$ motif at the chr4 *RFC1* locus using exSTRa identified an expansion of this STR only in CANVAS8, suggesting that this individual is a compound heterozygote, with an $(AAGGG)_{exp}$ RE on one allele and an $(AAAGG)_{exp}$ RE on the other. Visualization in IGV confirmed the presence of the $(AAAGG)_n$ motif embedded within the reference STR: $(AAAAG)_6$-$(AAAGG)_n$-$(AAAAG)_6$ (Figure S3). This observation raises the possibility that an expanded $(AAAGG)_{exp}$ motif might also be associated with CANVAS.

EH, TREDPARSE, and GangSTR were used to estimate the length of the AAGGG motif on each allele (Figure 3). The results were highly variable depending on the tool used. EH reported minimum and maximum allele sizes ranging from 30 to 68 in individuals with the RE. The allele size ranges estimated by GangSTR and TREPARSE were 2 to 27 and 7 to 14, respectively. Furthermore, all three tools inferred the presence of two alleles, even in individuals who carry a single allele, and hence do not appear to be distinguishing read contributions between the alleles, also contributing to unreliable size estimates. Reads comprised of the $(AAGGG)_{exp}$ motif in particular also showed evidence of high read sequencing error. Based on these results, we can infer that while the

CANVAS samples were all correctly identified as having homozygous RE at *RFC1*, estimates of expansion size are inconsistent and appear likely to significantly underestimate the actual repeat size.

The consensus of the different tools was that CANVAS11, 13, 17, and 19 families did not encode a pathogenic RE [either $(AAGGG)_{exp}$ or $(AAAGG)_{exp}$] at the *RFC1* locus, which we confirmed by PCR analyses (see below). However, the *RFC1* $(AAGGG)_{exp}$ RE was present in three of the control WGS datasets (two heterozygous, one homozygous, allele frequency ~0.06 [4/62]; Figure 3). No control individuals were identified to carry the $(AAAGG)_{exp}$ motif. As with the CANVAS samples, the STR sizing estimates using the different tools was inconsistent, so no conclusions could be drawn from this *in silico* analysis regarding the relative size of the $(AAGGG)_{exp}$ RE in control subjects compared to individuals with CANVAS. We then analyzed a larger in-house collection of unrelated control Coriell WGS samples (n = 69) and again failed to identify the $(AAAGG)_{exp}$ motif. However, we identified six individuals heterozygous for the $(AAGGG)_{exp}$ RE, representing a frequency estimate of ~0.04 (6/138; Figure S4). Using the NGS QC software tool peddy, we found evidence that two of these heterozygous individuals are of European ancestry and that two further individuals are of admixed Native American ancestry. Finally, we accessed WGS from GTEx for 133 individuals who have matching brain (cerebellum) RNA-seq. Our analysis identified 11 heterozygous carriers of the $(AAGGG)_{exp}$ RE, representing an estimated allele frequency of ~0.04 (11/266), consistent with our in-house collection.

Validation of the $(AAGGG)_n$ RE as the Causal Variant for CANVAS

We developed a PCR assay that amplifies across the repeat tract to rapidly screen for the presence of a non-expanded allele at the *RFC1* STR. Although the screen does not distinguish between the $(AAAAG)_{11}$ reference STR, the (AAGGG) STR, or any other potential motif, amplification of an ~250 bp fragment indicates at least one allele is not expanded. Moreover, the presence of two distinct non-expanded products is indicative of a heterozygous non-mutant state. Conversely, the complete absence of the PCR product provides indirect evidence of a RE affecting both alleles of the *RFC1* locus. Analysis of all available DNA samples from individuals with CANVAS suggested that the reference STR at the *RFC1* locus was not present in 30 clinically diagnosed individuals from 18 (of 22) CANVAS-affected families (Table 1, Figure 4). Notably, unaffected individuals from *RFC1*-positive families carried at least one non-expanded *RFC1* allele (Figure S5). To directly confirm expansion of the (AAGGG) motif in *RFC1*, we developed a locus-specific repeat-primed PCR assay, using a primer located adjacent to the *RFC1* repeat and an AAGGG-specific primer. Consistent with the PCR assay, affected individuals from the 18 families demonstrated a saw-toothed "ladder" when the repeat-primed PCR products were analyzed by capillary array (Table 1, Figure 4). These results suggest that a homozygous RE underlies CANVAS in these 18 families, and at least one pathogenic allele encodes the $(AAGGG)_{exp}$ RE. Molecular analysis of the DNA for the three in-house control individuals with the *in silico* predicted $(AAGGG)_{exp}$ motif (Figure 3) demonstrated a ~250 bp product in both heterozygous samples but no product in the homozygous individual. The repeat-primed assay demonstrated a saw-toothed ladder in all three samples (Figure S6). Collectively, these analyses suggested all three control individuals have at least one copy of the pathogenic $(AAGGG)_{exp}$ RE at *RFC1*, although the size of the RE cannot be determined by these analyses.

In four families (CANVAS11, 13, 17, and 19), the presence of the expected reference PCR amplicon and lack of a repeat-primed PCR product suggested that the pathogenic *RFC1* RE was not present on either allele. This implied that these individuals have a different CANVAS-causing mutation in *RFC1*, or there is locus heterogeneity. A third possibility is that they do not have CANVAS but instead a related ataxia. Therefore, we performed WGS on these individuals and initially screened for known REs associated with ataxias using exSTRa and EH. A CAG trinucleotide expansion in *ATXN3*, associated with spino-cerebellar ataxia type 3 (SCA3 [MIM: 109150], also known as Machado-Josephs disease) was identified in CANVAS13 (Figure S7) and confirmed by diagnostic testing. The WGS was then screened for unreported or rare SNPs and indels in genes known to cause ataxia. No *de novo* or rare variants were identified in *RFC1*, but a potential genomic re-diagnosis was achieved in two additional families. In CANVAS17, two variants (GenBank: NM_001278055; c.12398delT [p.Phe4133Serfs*28] and GenBank: NM_001278055; c.5306T>A [p.Val1769Asp]) were identified in the gene encoding sacsin (*SACS*) and segregation analysis confirmed they were in *trans*. Biallelic mutations in *SACS* cause spastic ataxia of the Charlevoix-Saguenay type (MIM: 270550). In CANVAS19, a heterozygous variant in the gene encoding FAT tumor suppressor homolog 2 (*FAT2*; GenBank: NM_001447.2; c.4370T>C [p.Val1457Ala]) was identified. Heterozygous mutations in *FAT2* have recently been associated with SCA45 (MIM: 604269).[45] No potentially pathogenic variants were identified in CANVAS11, but a variant of unknown significance was identified in the gene encoding Ataxin 7 (*ATXN7*; GenBank: NM_001177387.1; c.2827C>G [p.Arg943Gly]). CANVAS11 was also screened genome-wide with EHdn for potentially pathogenic unreported RE, but no additional candidate REs were identified.

A Single Founder Event for the $(AAGGG)_n$ RE in *RFC1*

We performed haplotype analysis to determine whether the $(AAGGG)_{exp}$ RE arose more than once in human history. Analysis of haplotypes inferred from the WES data identified a core ancestral haplotype, comprised of 27 SNPs (Figure 5A), that was shared by most individuals except CANVAS14 (Table 1, Table S4). The core haplotype

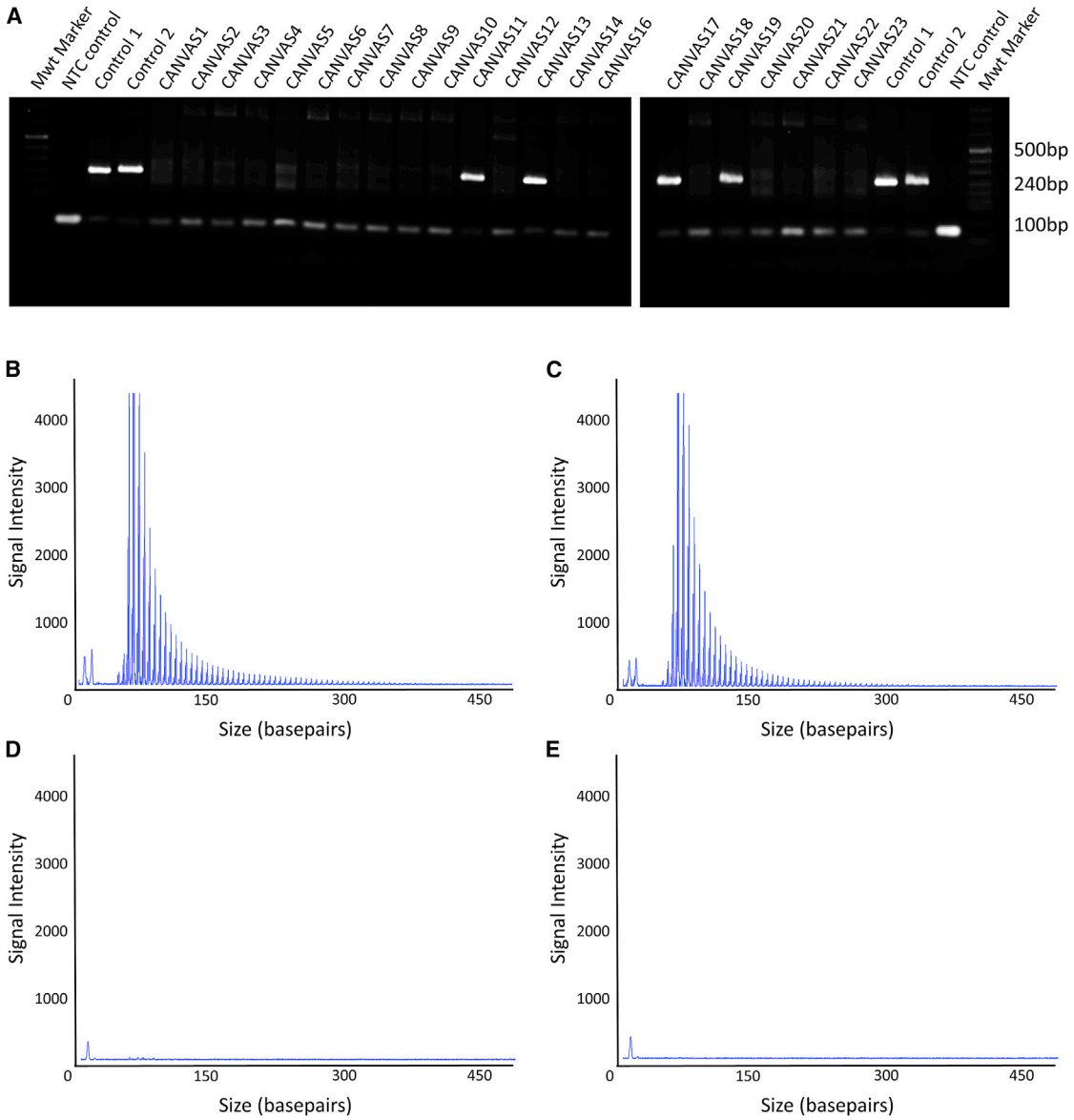

Figure 4. Genetic Validation of the $(AAGGG)_{exp}$ RE
(A) PCR analysis of the *RFC1* STR failed to produce the control ~253 bp reference product in 18 of 22 CANVAS-affected families.
(B and C) Representative images of the repeat-primed PCR for the $(AAGGG)_{exp}$ RE demonstrating a saw-toothed product with 5 base pair repeat unit size, amplified from gDNA of individuals from CANVAS1 (B) and CANVAS9 (C).
(D and E) No product was observed for the unaffected control (D) and no gDNA template negative control (E).

spans four genes (*TMEM156*, *KLHL5*, *WDR19*, and *RFC1*) and is 0.36 Mb in size (chr4:38995374–39353137, hg19). Inspection of this region in the UCSC browser suggested that the core haplotype overlaps with a region of strong linkage disequilibrium in European and Asian populations (Han Chinese and Japanese from Tokyo), but not the Yoruba population (an ethnic group from West Africa, Figure 5B). Using a DNA recombination and haplotype-based mutation dating technique,[42] we estimate that the most recent common ancestor (MRCA) of the CANVAS cohort lived approximately 25,880 (CI: 14,080–48,020) years ago (Figure 5C). This age estimate corresponds to the size of the haplotype and LD block and is roughly equivalent to the origin of modern Europeans as represented by the HAPMAP CEU cohort. Further investigation of the haplotypes allowed us to infer a simple phylogeny based on identified clusters of shared haplotypes extending beyond the core haplotype, suggesting that some individuals have common ancestors more recent than that of the MRCA for the whole group. This approach identified four subgroups. Group A had a MRCA dating back 5,600 (CI: 2,120–15,520) years and group B (further divided into groups B1 and B2) have a MRCA dating back 4,180 years (CI: 2,240–7,940). Furthermore, one individual shared part of their haplotype with both groups A and B, suggesting that group B is a distant branch of the MRCA of group A. Another subgroup, C, has a MRCA that lived 1,860 (CI: 560–7,020) years ago. The final group, labeled

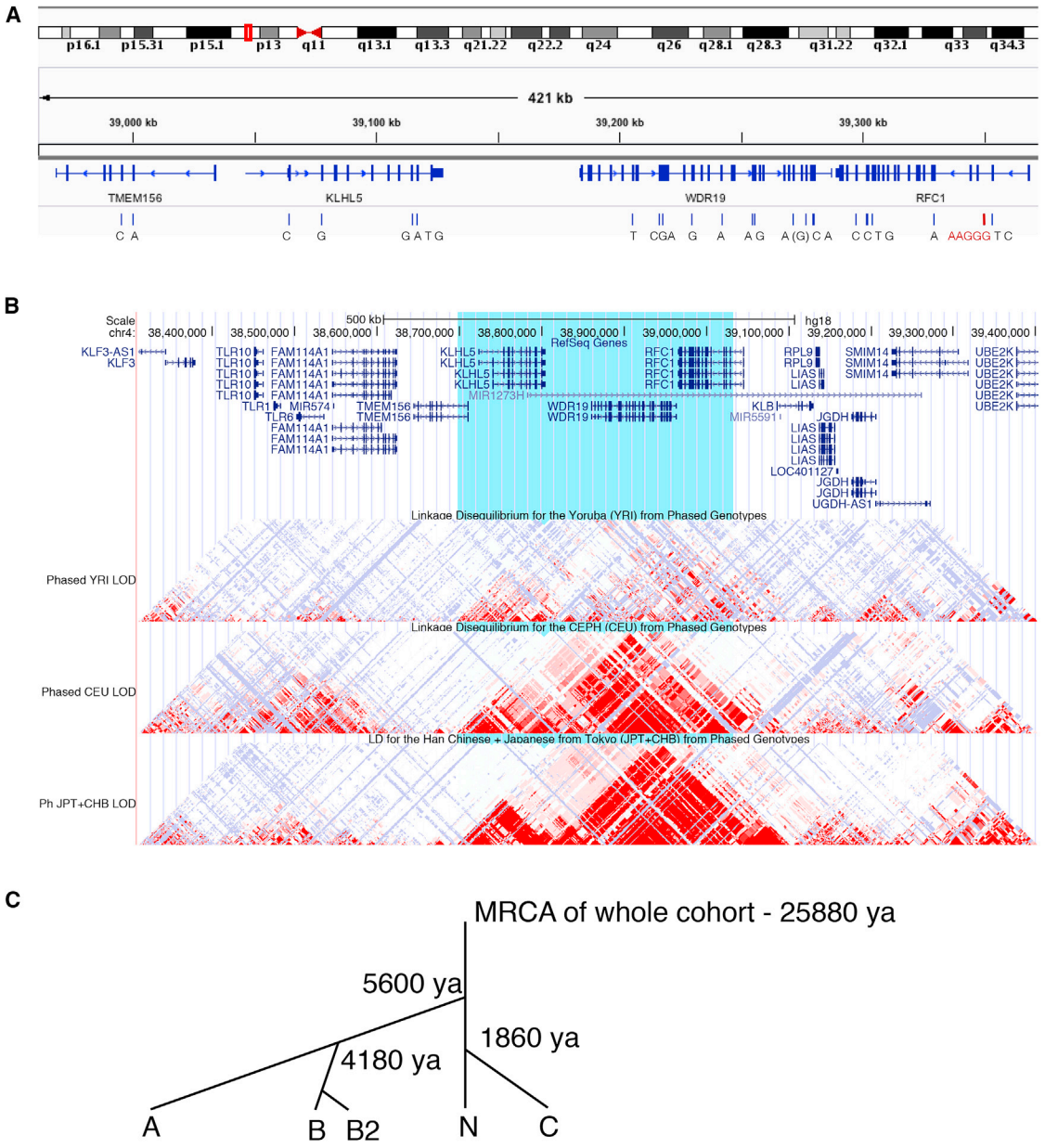

Figure 5. The Majority of Individuals with CANVAS Encode an Ancestral Haplotype

(A) Analysis of WES data identified an ancestral haplotype surrounding *RFC1* in all affected individuals confirmed to carry the $(AAGGG)_{exp}$ RE.

(B) The core haplotype (blue highlight) was intersected with the linkage disequilibrium (LD) track in the UCSC browser (converted to hg18 coordinates). The three LD tracks represent the Yoruba population (top track), Europeans (middle), and Han Chinese and Japanese from Tokyo (bottom). Red areas indicate strong linkage disequilibrium. The core CANVAS haplotype spans a large LD block in Europeans, which is broken up into two LD blocks in Japanese and Chinese, suggesting an ancient origin for the CANVAS repeat expansion allele.

(C) Haplotype sharing between individuals with CANVAS was used to determine the age of the most recent common ancestor (MRCA) of the cohort.

N, do not have any additional sharing beyond the core haplotype.

Next, we compared the haplotype of the nine control samples (three in-house control subjects and six from the Coriell collection) that carry the $(AAGGG)_{exp}$ RE to the core haplotype defined in the individuals with CANVAS. All control subjects shared at least part of the core haplotype, again suggesting that the $(AAGGG)_{exp}$ RE arose once in history. Finally, we determined that 9 of the 11 individuals from GTEx heterozygous for the $(AAGGG)_{exp}$ RE also shared the same core haplotype identified in individuals with CANVAS. The haplotype-specific SNP rs2066782 (exon 18, chr4:39303925, A>G) enabled us to analyze the expression of the $(AAGGG)_{exp}$ *RFC1* allele in the cerebellum RNA-seq data and confirm that the STR did not inhibit the expression of *RFC1* compared to the reference $(AAAAG)_{11}$ allele. The remaining two carriers do not appear to share the core haplotype. As they do

not have heterozygous SNPs in their exons, allele-specific expression could not be determined.

Discussion

Since the first description of the syndrome of cerebellar ataxia with bilateral vestibulopathy in 2004[46] and proposal of CANVAS as a distinct clinical entity in 2011,[11] there has been little progress made in delineating the etiology of the disorder. While most affected individuals are described as idiopathic, reports of multiple affected sib pairs[12] and a family with three affected individuals[47] have suggested that an autosomal-recessive mode of inheritance is most likely. The genetic basis of CANVAS has now been identified and validated in two independent studies, one recently published by Cortese et al.[32] and this study. Both studies utilized a similar study design, with linkage analysis to reduce the genomic search space to a modest interval (<2 Mb), but no plausible causal variant(s) could be identified in WES data. WGS was then performed on multiple individuals and Cortese et al.[32] successfully identified the RE by visual inspection of the aligned read pairs inside the linkage region using the Integrative Genomics Viewer. In contrast, we utilized a bioinformatics approach and performed genome-wide analysis of WGS data to identify potential RE and then prioritized the RE located within the linkage interval. While both approaches were successful, the bioinformatics approach to RE detection, as described in this study, is likely more sensitive and practical and can be applied even in the absence of a small, or indeed any, linkage region. Furthermore, using a bioinformatics approach allows simultaneous testing of other potentially causal RE due to differential diagnoses. For example, we quickly re-diagnosed an affected individual with a pathogenic SCA3 RE.

Previously, the only variant associated with CANVAS was a heterozygous missense variant in the gene encoding E74 Like ETS Transcription Factor 2 (*ELF2*), which segregated with the disorder in three individuals in a single family.[47] It is now apparent that the majority of individuals with CANVAS result from the homozygous inheritance of an expanded intronic pentamer in *RFC1*. We found the $(AAGGG)_{exp}$ in 30 of 31 individuals with a RE at this locus. In only a single individual did we observe a different, presumably pathogenic motif; CANVAS8 had one allele with the $(AAGGG)_{exp}$, whereas the second allele appeared to consist of an $(AAAGG)_{exp}$. Notably, this alternate motif does not share the AAGGG haplotype (Figure S3). Analysis of the core haplotype in the majority of individuals with CANVAS suggests that the $(AAGGG)_{exp}$ RE arose once, approximately 25,000 years ago, most likely in Europe. While the majority of individuals in our cohort who carry the $(AAGGG)_n$ RE are of European ancestry, the RE is also present in non-European individuals, including a Lebanese family and two carriers of admixed Native American ancestry. Given the age of the CANVAS RE and recent human admixture, it is likely that the locus may underlie CANVAS in apparently non-European individuals, despite the disorder being highly overrepresented in European populations.

Importantly, Cortese et al.[32] extend the clinical significance of the CANVAS RE by demonstrating it is potentially a common cause of unsolved ataxia not meeting the diagnostic criteria of CANVAS. Screening for homozygous inheritance of the $(AAGGG)_{exp}$ RE in a cohort of 150 individuals with sporadic late-onset ataxia diagnosed 33 individuals (22%). This is consistent with the relatively high allele frequency of the $(AAGGG)_{exp}$ we report in this paper. Collectively, the two studies screened for the RE in a total of 537 clinically normal samples, identifying 23 heterozygous and a single homozygous individual (allele frequency 25/1,074 = 0.023). Given that the allele size and RE composition could not be determined in all control subjects, it is possible that the unaffected homozygous individual we identified carries two alleles smaller than the pathogenic range of >400 repeats reported by Cortese et al.[32] However, the individual is less than half the mean age of CANVAS onset (~60 years) and the lack of phenotype suggests the clinical features are yet to manifest.

Mechanism of Pathogenicity

There are multiple mechanisms by which RE can lead to pathogenicity, including RNA toxicity, protein toxicity, and loss or gain of function.[7] It is not yet known how the $(AAGGG)_{exp}$ RE in *RFC1* causes CANVAS, but the homozygous inheritance pattern suggests a loss-of-function mechanism, rather than RNA or protein toxicity. In heterozygous carriers of the $(AAGGG)_{exp}$ RE, our analysis of the GTEx RNA-seq data using haplotype tagging SNPs suggested that the pathogenic $(AAGGG)_{exp}$ allele did not inhibit expression of *RFC1* compared to the reference $(AAAAG)_{11}$ allele. Interestingly, Cortese et al.[32] also were unable to determine a mechanism of action. The $(AAGGG)_{exp}$ RE did not appear to alter expression levels of *RFC1* or surrounding genes as determined by bulk RNA-seq and qRT-PCR. Similarly, *RFC1* expression and protein levels appeared unchanged in peripheral or brain tissue derived from individuals with CANVAS, and no AAGGG RNA foci deposits were observed.[32] While *RFC1* has not been previously associated with any disorder, it appears extremely intolerant to LoF (pLI = 0.97; observed/expected = 0.18, CI 0.12–0.31).[48] In addition, siblings in the families studied carried the pathogenic RE in a heterozygous state but did not manifest any signs of the disorder. This observation is analogous to Friedreich ataxia, a recessive genetic ataxia caused by loss of function (LoF) of FRDA due to a pathogenic intronic RE.

RFC1 encodes a subunit of replication factor C, a five-subunit protein complex required for DNA replication and repair. Analysis of the Genotype-Tissue Expression (GTEx) database demonstrated significant expression of *RFC1* in brain tissue, particularly the cerebellum. Replication factor C catalyzes opening the protein ring of proliferating cell nuclear antigen (PCNA), allowing it to encircle

the DNA and function as a scaffold to recruit proteins involved in DNA replication, repair, and remodeling.[49] Mutations in multiple DNA replication and repair genes such as *TCD1*, *PNKP*, *XRCC1*, and *APTX* result in ataxia,[50] highlighting the central role of this pathway in these overlapping disorders. One of the best-known examples is the severe and early-onset autosomal-recessive disorder ataxia telangiectasia, which is caused by mutations in the gene encoding ATM serine/threonine kinase (*ATM*), which is important for the repair of DNA double-strand breaks.[51]

The minimum pathogenic length and fine structure of the *RFC1* RE is currently unclear. While Cortese et al.[32] reported a pathogenic range of ~400–2,000, the individual repeat composition and a more precise repeat length was not determined. The short-read NGS technologies utilized in this study were unable to extend more than ~100 bp into the repeat sequence and efforts to amplify across the region using long-range PCR were unsuccessful. While the repeat-primed PCR assay indicates the presence of the $(AAGGG)_{exp}$ motif, it does not extend beyond ~250 bp (50 repeat units). The application of long-read sequencing technologies currently being developed for RE disorders will be required to accurately elucidate both the length of the pathogenic allele and the repeat composition. Both of these parameters provide important clinical information regarding onset, progression, and pathogenicity in other genetic ataxias such as SCA1 and Friedreich ataxia.[52,53] Additional studies will also be required to elucidate the nature of the *RFC1* STR in control individuals. Cortese et al.[32] demonstrated considerable variability is present in the size and composition of the STR, but details regarding the size and composition of both normal and pathogenic alleles are yet to be fully determined. We show that the $(AAGGG)_{exp}$ RE occurs within the 3′ end of the Alu element, AluSx3. Alu elements typically have A-rich tails and in the reference sequence the *RFC1* Alu has an A-rich tail containing an $(AAAAG)_{11}$ STR. There is some evidence that motifs that follow the pattern A_nG_m, especially $(AAAG)_n$ and $(AAAGG)_n$, display strong base-stacking interactions and are more likely to expand through replication slippage.[31] This suggests an inherent mitotic instability of A- and G-rich motifs, consistent with what we observe in CANVAS. Notably, a number of pathogenic RE located with Alu have previously been described, including SCA10, SCA31, SCA37, and Friedreich ataxia.[22,26,54,55]

Genomic Re-diagnosis in CANVAS

Of 22 families enrolled in this study with a clinical diagnosis of CANVAS, 4 did not harbor the RE or any other potentially pathogenic variants in the *RFC1* locus. CANVAS13 was re-diagnosed with SCA3 after the WGS data was analyzed using our computational pipeline for detecting known pathogenic REs. In addition to cerebellar ataxia, individuals with SCA3 not uncommonly manifests a somatosensory impairment[56,57] and vestibular involvement may be variably present,[57] resulting in a phenotype indistinguishable from CANVAS.[43] This molecular re-diagnosis highlights the power of modern STR detection techniques to diagnose RE ataxias. In addition, NGS data provide the opportunity to simultaneously identify non-RE-mediated causes of ataxia. In CANVAS17 we identified biallelic variants in *SACS* as the likely cause of disease. While individuals with spastic ataxia of the Charlevoix-Saguenay type may present with the combination of cerebellar ataxia and a peripheral neuropathy[58,59] as seen in CANVAS, to our knowledge vestibular involvement has not previously been described, and so this potentially constitutes a previously undescribed manifestation of the disease. In addition, a very plausible heterozygous variant was identified in *FAT2* in CANVAS19. While classified as a VUS using ACMG guidelines,[60] the variant is observed only once in gnomAD and was predicted pathogenic by multiple *in silico* algorithms. Very recently, heterozygous point mutations affecting the last cadherin domain (p.Lys3586Asn) or the linker region (p.Arg3649Gln) of *FAT2* have been associated with SCA45, adding weight to classifying the variant (p.Val1457Ala) in the 13th cadherin domain, as likely pathogenic. While the published clinical phenotype and mutation spectrum in SCA45 is limited, in common with CANVAS, it is a late-onset and slowly progressive cerebellar ataxia.[45]

Strengths and Limitations of Current STR Detection Tools

In this study, we implemented multiple computational tools to identify and validate the presence of an $(AAGGG)_{exp}$ RE in the majority of individuals with a clinical diagnosis of CANVAS. In particular, the use of EHdn, with its non-reference based RE discovery framework, was crucial in identifying a putative candidate, with the reference-based STR detection tools facilitating the follow-up analysis. Although all tools gave highly variable estimated repeat sizes, which are likely to be significantly less than the actual repeat size, they provided consistent evidence that the (AAGGG) motif was expanded. This level of evidence is helpful before embarking on the potentially complex process of molecular validation. In our analysis, only a single tool (GangSTR) failed to detect the alternate $(AAAGG)_{exp}$ RE. It is not clear why this was the case, although it could be related to the more complicated $[(AAAAG)_6\text{-}(AAAGG)_{exp}\text{-}(AAAAG)_6]$ repeat structure. Notably, EHdn was able to identify the $(AAAGG)_{exp}$ RE in CANVAS8-8, but genome-wide significance was not achieved and the motif was less highly ranked based on p value than the initial discovery of AAGGG (Table S3). This is likely due to the fact that power was reduced as there was only a single case subject and a small number of control subjects. EHdn appears most effective as a discovery tool when used with multiple case subjects or larger numbers of control subjects. The results of this study highlight the importance of utilizing multiple tools to provide

redundancy in the data analysis pipeline. We have now updated the exSTRa package (see Web Resources below) to include CANVAS and other recently described pathogenic RE, providing additional utility to the research community to rapidly identify these RE in their cohorts. An additional issue we encountered, which potentially limited all tools, was the poor sequencing quality in reads containing the (AAGGG) motif compared to other STRs.

In conclusion, in this study we show that a recessively inherited, ancient RE located in intron 2 of *RFC1* is the predominant cause of CANVAS. Recently developed RE discovery tools facilitated the identification and verification of this previously undescribed RE, in addition to identifying other genetic causes of disease in the cohort. Despite the RE being located in an intron, we demonstrate that previously generated WES data with low-coverage genome-wide off target reads were helpful in providing increased statistical confidence in RE identification. Therefore, reanalysis of previously generated WES datasets potentially offers a cost-effective approach to facilitate identification of intronic RE, not currently described in the genome reference sequence, in discovery projects. Finally, we anticipate that implementation of these tools into routine diagnostic pipelines has the potential to significantly increase the current diagnostic rates of <40%, recorded for clinical exome and targeted panel analyses of individuals with ataxia.[61,62]

Data and Code Availability

The ClinVar details for the *RFC1* variants reported in this paper are SCV000898492.1 and SCV000898493.1.

Supplemental Data

Supplemental Data can be found online at https://doi.org/10.1016/j.ajhg.2019.05.016.

Acknowledgments

We acknowledge access to the dataset EGA00001003562 from the European Genome-Phenome Archive. This work was supported by the Australian Government National Health and Medical Research Council (Program Grant 1054618 to M.B.), the NIH (NINDS grant R01NS082094 to B.L.F.), and the Murdoch Children's Research Institute. M.B. was supported by an NHMRC Senior Research Fellowship (1102971) and D.P.B. was supported by a Wellcome Clinical Research Career Development Fellowship. Additional funding was provided by the Independent Research Institute Infrastructure Support Scheme and the Victorian State Government Operational Infrastructure Program.

Declaration of Interests

The authors declare no conflicts of interest.

Received: February 27, 2019
Accepted: May 21, 2019
Published: June 20, 2019

Web Resources

Bird, T.D. (2018). Hereditary Ataxia Overview. In GeneReviews, https://www.ncbi.nlm.nih.gov/books/NBK1138/
Cavalier, https://github.com/bahlolab/cavalier
ClinVar, https://www.ncbi.nlm.nih.gov/clinvar/
European Genome-phenome Archive (EGA), https://www.ebi.ac.uk/ega
exSTRa, https://github.com/bahlolab/exSTRa
GenBank, https://www.ncbi.nlm.nih.gov/genbank/
gnomAD Browser, https://gnomad.broadinstitute.org/
GTEx Portal, https://gtexportal.org/home/
IGV, http://www.broadinstitute.org/igv/
Mutation dating, https://shiny.wehi.edu.au/rafehi.h/mutation-dating/
OMIM, https://www.omim.org/
UCSC Genome Browser, https://genome.ucsc.edu
Varsome, https://varsome.com

References

1. McMurray, C.T. (2010). Mechanisms of trinucleotide repeat instability during human development. Nat. Rev. Genet. *11*, 786–799.
2. Gymrek, M., Willems, T., Guilmatre, A., Zeng, H., Markus, B., Georgiev, S., Daly, M.J., Price, A.L., Pritchard, J.K., Sharp, A.J., and Erlich, Y. (2016). Abundant contribution of short tandem repeats to gene expression variation in humans. Nat. Genet. *48*, 22–29.
3. Quilez, J., Guilmatre, A., Garg, P., Highnam, G., Gymrek, M., Erlich, Y., Joshi, R.S., Mittelman, D., and Sharp, A.J. (2016). Polymorphic tandem repeats within gene promoters act as modifiers of gene expression and DNA methylation in humans. Nucleic Acids Res. *44*, 3750–3762.
4. Benson, G. (1999). Tandem repeats finder: a program to analyze DNA sequences. Nucleic Acids Res. *27*, 573–580.
5. Subramanian, S., Madgula, V.M., George, R., Mishra, R.K., Pandit, M.W., Kumar, C.S., and Singh, L. (2003). Triplet repeats in human genome: distribution and their association with genes and other genomic regions. Bioinformatics *19*, 549–552.
6. La Spada, A.R., and Taylor, J.P. (2010). Repeat expansion disease: progress and puzzles in disease pathogenesis. Nat. Rev. Genet. *11*, 247–258.
7. Hannan, A.J. (2018). Tandem repeats mediating genetic plasticity in health and disease. Nat. Rev. Genet. *19*, 286–298.
8. Tankard, R.M., Bennett, M.F., Degorski, P., Delatycki, M.B., Lockhart, P.J., and Bahlo, M. (2018). Detecting Expansions of Tandem Repeats in Cohorts Sequenced with Short-Read Sequencing Data. Am. J. Hum. Genet. *103*, 858–873.
9. Ruano, L., Melo, C., Silva, M.C., and Coutinho, P. (2014). The global epidemiology of hereditary ataxia and spastic paraplegia: a systematic review of prevalence studies. Neuroepidemiology *42*, 174–183.
11. Szmulewicz, D.J., Waterston, J.A., Halmagyi, G.M., Mossman, S., Chancellor, A.M., McLean, C.A., and Storey, E. (2011). Sensory neuropathy as part of the cerebellar ataxia neuropathy vestibular areflexia syndrome. Neurology *76*, 1903–1910.
12. Szmulewicz, D.J., McLean, C.A., MacDougall, H.G., Roberts, L., Storey, E., and Halmagyi, G.M. (2014). CANVAS an update: clinical presentation, investigation and management. J. Vestib. Res. *24*, 465–474.

13. Harding, A.E. (1981). "Idiopathic" late onset cerebellar ataxia. A clinical and genetic study of 36 cases. J. Neurol. Sci. *51*, 259–271.
14. Szmulewicz, D.J. (2017). Combined Central and Peripheral Degenerative Vestibular Disorders: CANVAS, Idiopathic Cerebellar Ataxia with Bilateral Vestibulopathy (CABV) and Other Differential Diagnoses of the CABV Phenotype. Curr. Otorhinolaryngol. Rep. *5*, 167–174.
15. Cha, Y.H. (2012). Less common neuro-otologic disorders. Continuum (Minneap. Minn.) *18* (5 Neuro-otology), 1142–1157.
16. Szmulewicz, D.J., Merchant, S.N., and Halmagyi, G.M. (2011). Cerebellar ataxia with neuropathy and bilateral vestibular areflexia syndrome: a histopathologic case report. Otol. Neurotol. *32*, e63–e65.
17. Szmulewicz, D.J., McLean, C.A., Rodriguez, M.L., Chancellor, A.M., Mossman, S., Lamont, D., Roberts, L., Storey, E., and Halmagyi, G.M. (2014). Dorsal root ganglionopathy is responsible for the sensory impairment in CANVAS. Neurology *82*, 1410–1415.
18. Szmulewicz, D.J., Seiderer, L., Halmagyi, G.M., Storey, E., and Roberts, L. (2015). Neurophysiological evidence for generalized sensory neuronopathy in cerebellar ataxia with neuropathy and bilateral vestibular areflexia syndrome. Muscle Nerve *51*, 600–603.
19. Szmulewicz, D.J., Waterston, J.A., MacDougall, H.G., Mossman, S., Chancellor, A.M., McLean, C.A., Merchant, S., Patrikios, P., Halmagyi, G.M., and Storey, E. (2011). Cerebellar ataxia, neuropathy, vestibular areflexia syndrome (CANVAS): a review of the clinical features and video-oculographic diagnosis. Ann. N Y Acad. Sci. *1233*, 139–147.
20. Petersen, J.A., Wichmann, W.W., and Weber, K.P. (2013). The pivotal sign of CANVAS. Neurology *81*, 1642–1643.
21. Szmulewicz, D., MacDougall, H., Storey, E., Curthoys, I., and Halmagyi, M. (2014). A Novel Quantitative Bedside Test of Balance Function: The Video Visually Enhanced Vestibulo-ocular Reflex (VVOR). Neurology *82*, S19.
22. Campuzano, V., Montermini, L., Moltò, M.D., Pianese, L., Cossée, M., Cavalcanti, F., Monros, E., Rodius, F., Duclos, F., Monticelli, A., et al. (1996). Friedreich's ataxia: autosomal recessive disease caused by an intronic GAA triplet repeat expansion. Science *271*, 1423–1427.
23. Taki, M., Nakamura, T., Matsuura, H., Hasegawa, T., Sakaguchi, H., Morita, K., Ishii, R., Mizuta, I., Kasai, T., Mizuno, T., and Hirano, S. (2018). Cerebellar ataxia with neuropathy and vestibular areflexia syndrome (CANVAS). Auris Nasus Larynx *45*, 866–870.
24. Maruta, K., Aoki, M., and Sonoda, Y. (2019). [Cerebellar ataxia with neuropathy and vestibular areflexia syndrome (CANVAS): a case report]. Rinsho Shinkeigaku *59*, 27–32.
25. Bahlo, M., Bennett, M.F., Degorski, P., Tankard, R.M., Delatycki, M.B., and Lockhart, P.J. (2018). Recent advances in the detection of repeat expansions with short-read next-generation sequencing. F1000Res. *7*, 7.
26. Seixas, A.I., Loureiro, J.R., Costa, C., Ordóñez-Ugalde, A., Marcelino, H., Oliveira, C.L., Loureiro, J.L., Dhingra, A., Brandão, E., Cruz, V.T., et al. (2017). A Pentanucleotide ATTTC Repeat Insertion in the Non-coding Region of DAB1, Mapping to SCA37, Causes Spinocerebellar Ataxia. Am. J. Hum. Genet. *101*, 87–103.
27. Ishiura, H., Doi, K., Mitsui, J., Yoshimura, J., Matsukawa, M.K., Fujiyama, A., Toyoshima, Y., Kakita, A., Takahashi, H., Suzuki, Y., et al. (2018). Expansions of intronic TTTCA and TTTTA repeats in benign adult familial myoclonic epilepsy. Nat. Genet. *50*, 581–590.
28. Dolzhenko, E., van Vugt, J.J.F.A., Shaw, R.J., Bekritsky, M.A., van Blitterswijk, M., Narzisi, G., Ajay, S.S., Rajan, V., Lajoie, B.R., Johnson, N.H., et al.; US–Venezuela Collaborative Research Group (2017). Detection of long repeat expansions from PCR-free whole-genome sequence data. Genome Res. *27*, 1895–1903.
29. Tang, H., Kirkness, E.F., Lippert, C., Biggs, W.H., Fabani, M., Guzman, E., Ramakrishnan, S., Lavrenko, V., Kakaradov, B., Hou, C., et al. (2017). Profiling of Short-Tandem-Repeat Disease Alleles in 12,632 Human Whole Genomes. Am. J. Hum. Genet. *101*, 700–715.
30. Dashnow, H., Lek, M., Phipson, B., Halman, A., Sadedin, S., Lonsdale, A., Davis, M., Lamont, P., Clayton, J.S., Laing, N.G., et al. (2018). STRetch: detecting and discovering pathogenic short tandem repeat expansions. Genome Biol. *19*, 121.
31. Mousavi, N., Shleizer-Burko, S., and Gymrek, M. (2018). Profiling the genome-wide landscape of tandem repeat expansions. bioRxiv. https://doi.org/10.1101/361162.
32. Cortese, A., Simone, R., Sullivan, R., Vandrovcova, J., Tariq, H., Yau, W.Y., Humphrey, J., Jaunmuktane, Z., Sivakumar, P., Polke, J., et al. (2019). Biallelic expansion of an intronic repeat in RFC1 is a common cause of late-onset ataxia. Nat. Genet. *51*, 649–658.
33. Smith, K.R., Bromhead, C.J., Hildebrand, M.S., Shearer, A.E., Lockhart, P.J., Najmabadi, H., Leventer, R.J., McGillivray, G., Amor, D.J., Smith, R.J., and Bahlo, M. (2011). Reducing the exome search space for mendelian diseases using genetic linkage analysis of exome genotypes. Genome Biol. *12*, R85.
34. Bahlo, M., and Bromhead, C.J. (2009). Generating linkage mapping files from Affymetrix SNP chip data. Bioinformatics *25*, 1961–1962.
35. Abecasis, G.R., Cherny, S.S., Cookson, W.O., and Cardon, L.R. (2002). Merlin–rapid analysis of dense genetic maps using sparse gene flow trees. Nat. Genet. *30*, 97–101.
36. Quinlan, A.R., and Hall, I.M. (2010). BEDTools: a flexible suite of utilities for comparing genomic features. Bioinformatics *26*, 841–842.
37. Pedersen, B.S., Layer, R.M., and Quinlan, A.R. (2016). Vcfanno: fast, flexible annotation of genetic variants. Genome Biol. *17*, 118.
38. Wang, K., Li, M., and Hakonarson, H. (2010). ANNOVAR: functional annotation of genetic variants from high-throughput sequencing data. Nucleic Acids Res. *38*, e164.
39. Dobin, A., Davis, C.A., Schlesinger, F., Drenkow, J., Zaleski, C., Jha, S., Batut, P., Chaisson, M., and Gingeras, T.R. (2013). STAR: ultrafast universal RNA-seq aligner. Bioinformatics *29*, 15–21.
40. Liao, Y., Smyth, G.K., and Shi, W. (2014). featureCounts: an efficient general purpose program for assigning sequence reads to genomic features. Bioinformatics *30*, 923–930.
41. Ritchie, M.E., Phipson, B., Wu, D., Hu, Y., Law, C.W., Shi, W., and Smyth, G.K. (2015). limma powers differential expression analyses for RNA-sequencing and microarray studies. Nucleic Acids Res. *43*, e47.
42. Gandolfo, L.C., Bahlo, M., and Speed, T.P. (2014). Dating rare mutations from small samples with dense marker data. Genetics *197*, 1315–1327.
43. Szmulewicz, D.J., Roberts, L., McLean, C.A., MacDougall, H.G., Halmagyi, G.M., and Storey, E. (2016). Proposed diagnostic criteria for cerebellar ataxia with neuropathy and

vestibular areflexia syndrome (CANVAS). Neurol. Clin. Pract. *6*, 61–68.
44. Wang, K., Li, M., Hadley, D., Liu, R., Glessner, J., Grant, S.F., Hakonarson, H., and Bucan, M. (2007). PennCNV: an integrated hidden Markov model designed for high-resolution copy number variation detection in whole-genome SNP genotyping data. Genome Res. *17*, 1665–1674.
45. Nibbeling, E.A.R., Duarri, A., Verschuuren-Bemelmans, C.C., Fokkens, M.R., Karjalainen, J.M., Smeets, C.J.L.M., de Boer-Bergsma, J.J., van der Vries, G., Dooijes, D., Bampi, G.B., et al. (2017). Exome sequencing and network analysis identifies shared mechanisms underlying spinocerebellar ataxia. Brain *140*, 2860–2878.
46. Rinne, T., Bronstein, A.M., Rudge, P., Gresty, M.A., and Luxon, L.M. (1998). Bilateral loss of vestibular function: clinical findings in 53 patients. J. Neurol. *245*, 314–321.
47. Ahmad, H., Requena, T., Frejo, L., Cobo, M., Gallego-Martinez, A., Martin, F., Lopez-Escamez, J.A., and Bronstein, A.M. (2018). Clinical and Functional Characterization of a Missense *ELF2* Variant in a CANVAS Family. Front. Genet. *9*, 85.
48. Lek, M., Karczewski, K.J., Minikel, E.V., Samocha, K.E., Banks, E., Fennell, T., O'Donnell-Luria, A.H., Ware, J.S., Hill, A.J., Cummings, B.B., et al.; Exome Aggregation Consortium (2016). Analysis of protein-coding genetic variation in 60,706 humans. Nature *536*, 285–291.
49. Zhang, G., Gibbs, E., Kelman, Z., O'Donnell, M., and Hurwitz, J. (1999). Studies on the interactions between human replication factor C and human proliferating cell nuclear antigen. Proc. Natl. Acad. Sci. USA *96*, 1869–1874.
50. Yoon, G., and Caldecott, K.W. (2018). Nonsyndromic cerebellar ataxias associated with disorders of DNA single-strand break repair. Handb. Clin. Neurol. *155*, 105–115.
51. Savitsky, K., Bar-Shira, A., Gilad, S., Rotman, G., Ziv, Y., Vanagaite, L., Tagle, D.A., Smith, S., Uziel, T., Sfez, S., et al. (1995). A single ataxia telangiectasia gene with a product similar to PI-3 kinase. Science *268*, 1749–1753.
52. Kraus-Perrotta, C., and Lagalwar, S. (2016). Expansion, mosaicism and interruption: mechanisms of the CAG repeat mutation in spinocerebellar ataxia type 1. Cerebellum Ataxias *3*, 20.
53. Mateo, I., Llorca, J., Volpini, V., Corral, J., Berciano, J., and Combarros, O. (2003). GAA expansion size and age at onset of Friedreich's ataxia. Neurology *61*, 274–275.
54. Bushara, K., Bower, M., Liu, J., McFarland, K.N., Landrian, I., Hutter, D., Teive, H.A., Rasmussen, A., Mulligan, C.J., and Ashizawa, T. (2013). Expansion of the Spinocerebellar ataxia type 10 (SCA10) repeat in a patient with Sioux Native American ancestry. PLoS ONE *8*, e81342.
55. Sato, N., Amino, T., Kobayashi, K., Asakawa, S., Ishiguro, T., Tsunemi, T., Takahashi, M., Matsuura, T., Flanigan, K.M., Iwasaki, S., et al. (2009). Spinocerebellar ataxia type 31 is associated with "inserted" penta-nucleotide repeats containing (TGGAA)n. Am. J. Hum. Genet. *85*, 544–557.
56. Jardim, L.B., Pereira, M.L., Silveira, I., Ferro, A., Sequeiros, J., and Giugliani, R. (2001). Neurologic findings in Machado-Joseph disease: relation with disease duration, subtypes, and (CAG)n. Arch. Neurol. *58*, 899–904.
57. Gordon, C.R., Zivotofsky, A.Z., and Caspi, A. (2014). Impaired vestibulo-ocular reflex (VOR) in spinocerebellar ataxia type 3 (SCA3): bedside and search coil evaluation. J. Vestib. Res. *24*, 351–355.
58. Gagnon, C., Desrosiers, J., and Mathieu, J. (2004). Autosomal recessive spastic ataxia of Charlevoix-Saguenay: upper extremity aptitudes, functional independence and social participation. Int. J. Rehabil. Res. *27*, 253–256.
59. Vill, K., Müller-Felber, W., Gläser, D., Kuhn, M., Teusch, V., Schreiber, H., Weis, J., Klepper, J., Schirmacher, A., Blaschek, A., et al. (2018). SACS variants are a relevant cause of autosomal recessive hereditary motor and sensory neuropathy. Hum. Genet. *137*, 911–919.
60. Richards, S., Aziz, N., Bale, S., Bick, D., Das, S., Gastier-Foster, J., Grody, W.W., Hegde, M., Lyon, E., Spector, E., et al.; ACMG Laboratory Quality Assurance Committee (2015). Standards and guidelines for the interpretation of sequence variants: a joint consensus recommendation of the American College of Medical Genetics and Genomics and the Association for Molecular Pathology. Genet. Med. *17*, 405–424.
61. Sullivan, R., Yau, W.Y., O'Connor, E., and Houlden, H. (2019). Spinocerebellar ataxia: an update. J. Neurol. *266*, 533–544.
62. Galatolo, D., Tessa, A., Filla, A., and Santorelli, F.M. (2018). Clinical application of next generation sequencing in hereditary spinocerebellar ataxia: increasing the diagnostic yield and broadening the ataxia-spasticity spectrum. A retrospective analysis. Neurogenetics *19*, 1–8.

The American Journal of Human Genetics, Volume *105*

Supplemental Data

Bioinformatics-Based Identification of Expanded Repeats: A Non-reference Intronic Pentamer Expansion in *RFC1* Causes CANVAS

Haloom Rafehi, David J. Szmulewicz, Mark F. Bennett, Nara L.M. Sobreira, Kate Pope, Katherine R. Smith, Greta Gillies, Peter Diakumis, Egor Dolzhenko, Michael A. Eberle, María García Barcina, David P. Breen, Andrew M. Chancellor, Phillip D. Cremer, Martin B. Delatycki, Brent L. Fogel, Anna Hackett, G. Michael Halmagyi, Solange Kapetanovic, Anthony Lang, Stuart Mossman, Weiyi Mu, Peter Patrikios, Susan L. Perlman, Ian Rosemergy, Elsdon Storey, Shaun R.D. Watson, Michael A. Wilson, David S. Zee, David Valle, David J. Amor, Melanie Bahlo, and Paul J. Lockhart

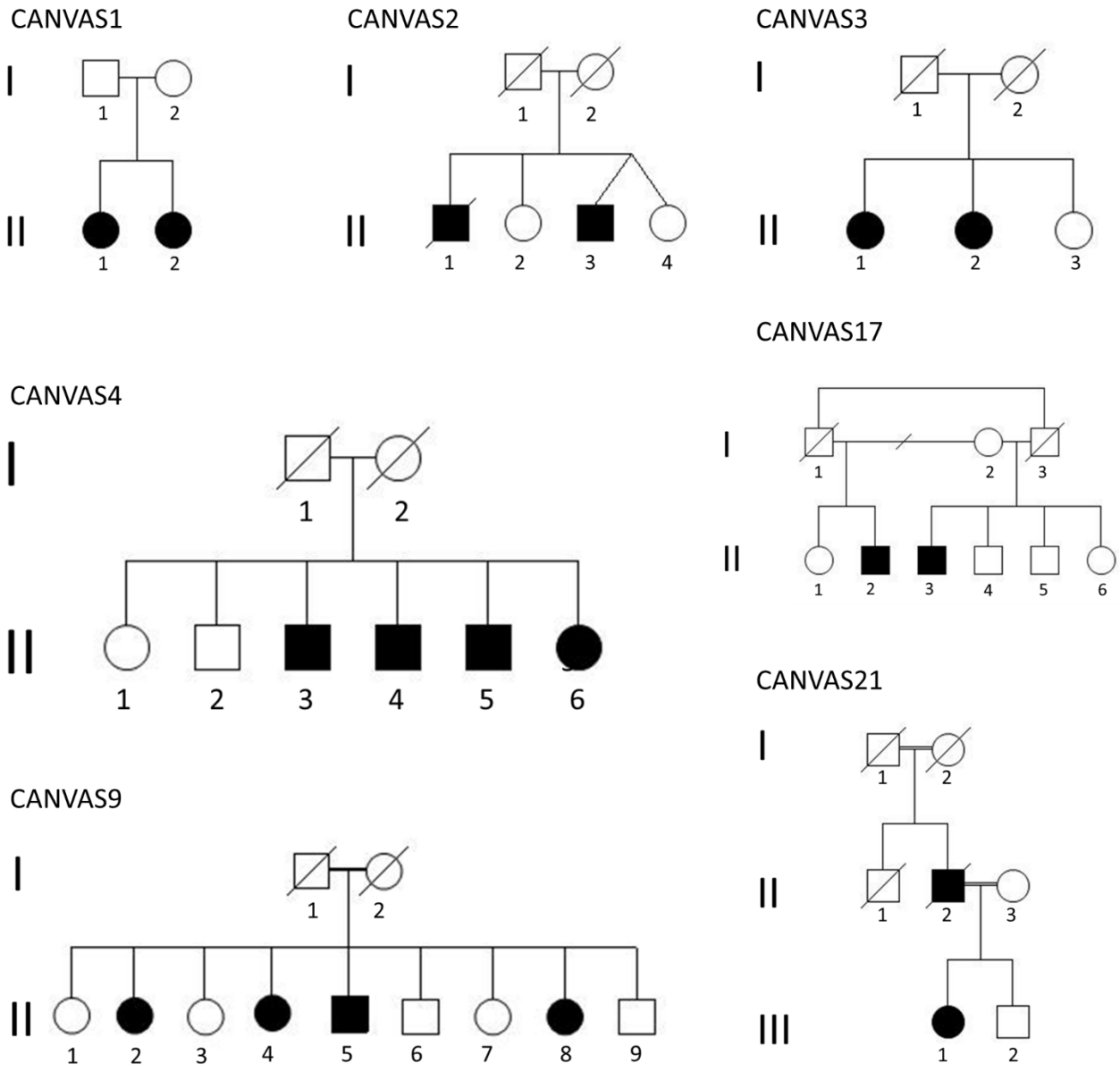

Figure S1: Pedigree structure of CANVAS families utilized for linkage studies (CANVAS1, 2, 3, 4 and 9) or demonstrating multigenerational inheritance.

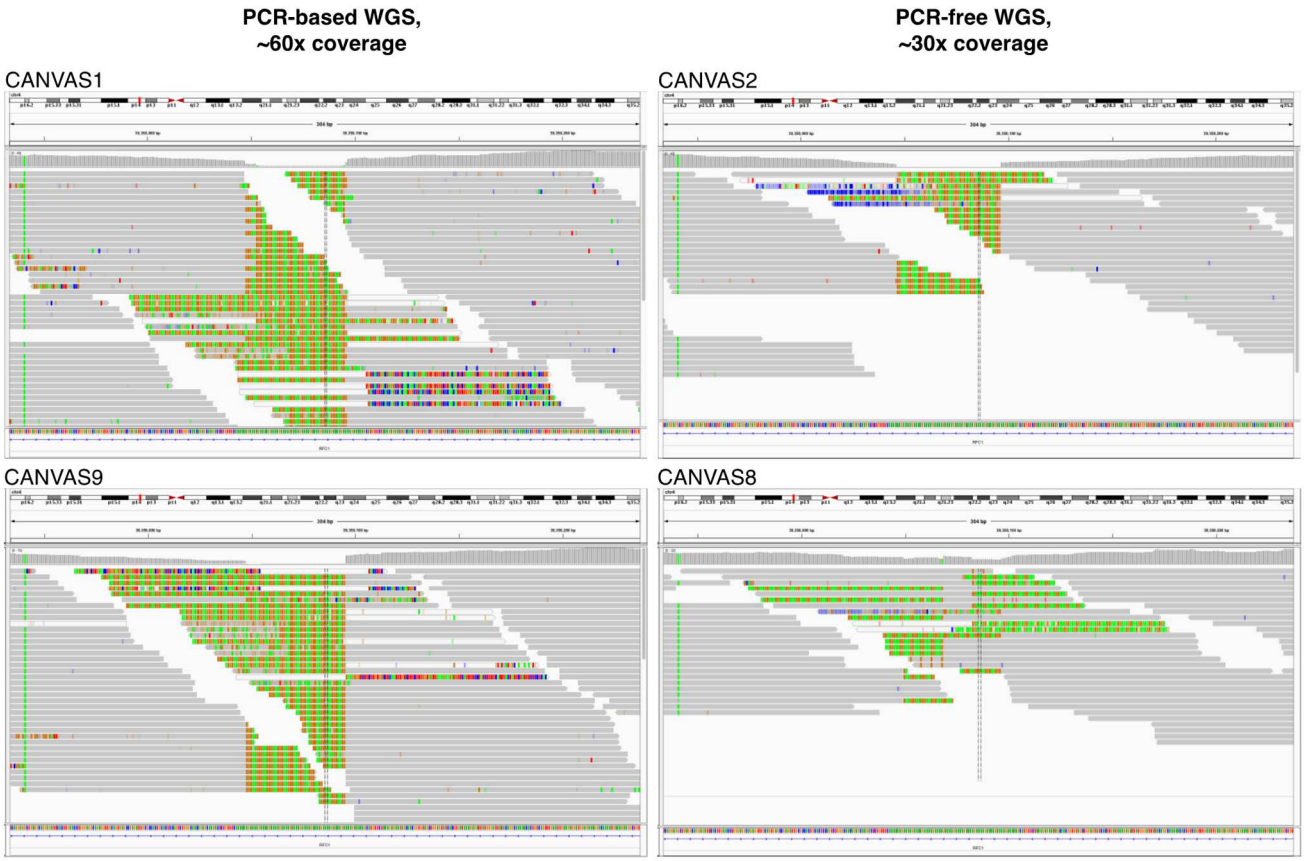

Figure S2: IGV snapshots of the (AAGGG)n locus in *RFC1*.

Illustrated are affected individuals from homozygous carriers of AAGGG (CANVAS1, 2, 9) and an individual who carries the AAGGG allele in addition to an expanded AAAGG allele (CANVAS8).

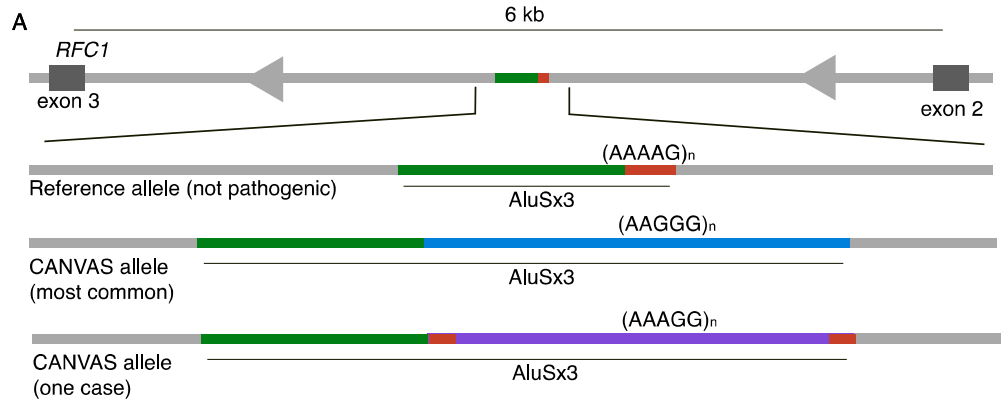

B

Individual ID	Allele	Pathogenic Motif	
REFERENCE			GACTCTGTTTCAAAAAAGAAAAGAAAAGAAAAGAAAAGAAAAGAAAAGAAAAGAAAAG--AAAAGAAAAGAAAAGAAAAGAAAAGAAAAGAAAAGAAAAGAAAAAGCAT
CANVAS9-10	A1/2	AAGGG	GACTCTGTTTCAAAAAGGGAAGGGAAGGGAAGGGAAGGGAAGGGAAGGGAAGGGAAGGG---AAGGGAAGGGAAGGGAAGGGAAGGGAAGGGAAGGGAAGAAAAAGCAT
CANVAS8-8	A1	AAGGG	GACTCTGTTTCAAAAAGGAAGGGAAGGGAAGGGAAGGGAAGGGAAGGGAAGGGAAGGG---AAGGGAAGGGAAGGGAAGGGAAGGGAAGGGAAGGGAAGAAAAAGCAT
CANVAS8-8	A2	AAAGG	GACTCTGTTTCAAAAAGAAAAGAAAAGAAAAGAAAAGAAAAGAAAAGAAAAGAAAAG--AAAGGAAAAGAAAAGAAAAGAAAAGAAAAGAAAAGAAAAGAAAAAGCAT
CANVAS2-2	A1	AAGGG	GACTCTGTTTCAAAAGGAAAGGGAAGGGAAGGGAAGGGAAGGGAAGGGAAGGGAAGGG----AAGGGAAGGGAAGGGAAGGGAAGGGAAGGGAAGGGAAGAAAAAGCAT
CANVAS2-2	A2	AAGGG	GACTCTGTTTCAAAAGGAAAGGAAAGGGAAGGGAAGGGAAGGGAAGGGAAGGGAAGGG----AAGGGAAGGGAAGGGAAGGGAAGGGAAGGGAAGGGAAGAAAAAGCAT
CANVAS1-1	A1	AAGGG	GACTCTGTTTCAAAAAAGAAGGGAAGGGAAGGGAAGGGAAGGGAAGGGAAGGGAAGGG---AAGGGAAGGGAAGGGAAGGGAAGGGAAGGGAAGGGAAGAAAAAGCAT
CANVAS1-1	A2	AAGGG	GACTCTGTTTCAAAAAGGGAAGGGAAGGGAAGGGAAGGGAAGGGAAGGGAAGGG---AAGGGAAGGGAAGGGAAGGGAAGGGAAGGGAAGGGAAGAAAAAGCAT

Figure S3: Schematic representation of pathogenic CANVAS alleles.

(A) Visual representation of the AAGGG and AAAGG repeat expansions in the second intron of *RFC1*. (B) Visual representation of the different AAGGG/AAAGG alleles in affected individuals identified by WGS.

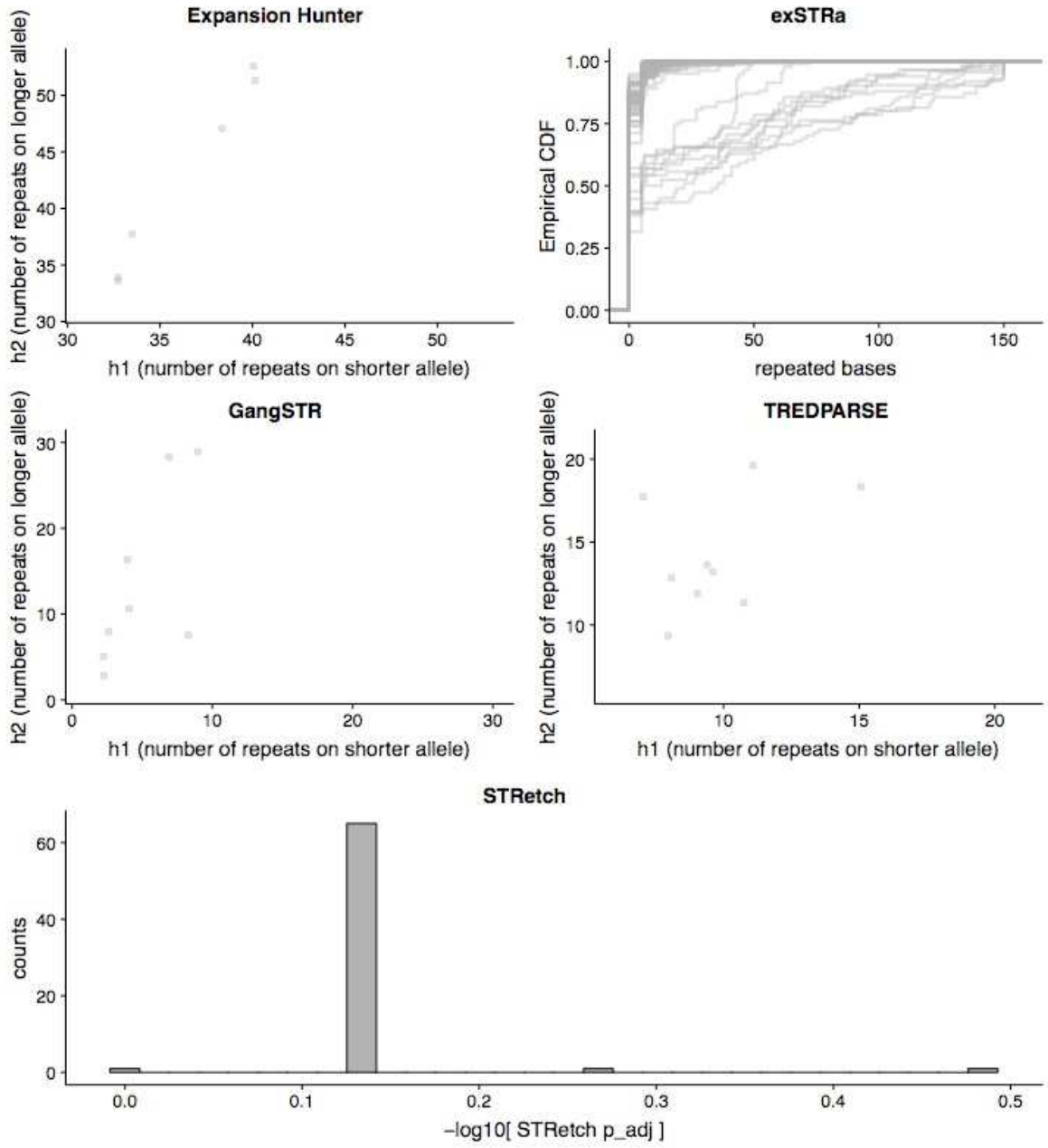

Figure S4: Computational validation of the $(AAGGG)_n$ STR.

The WGS from 69 unrelated non-CANVAS individuals (Coriell dataset) were analysed at the coordinate's chr4:39350045-39350095, using the tools exSTRa, EH, GangSTR, TREDPARSE and STRetch.

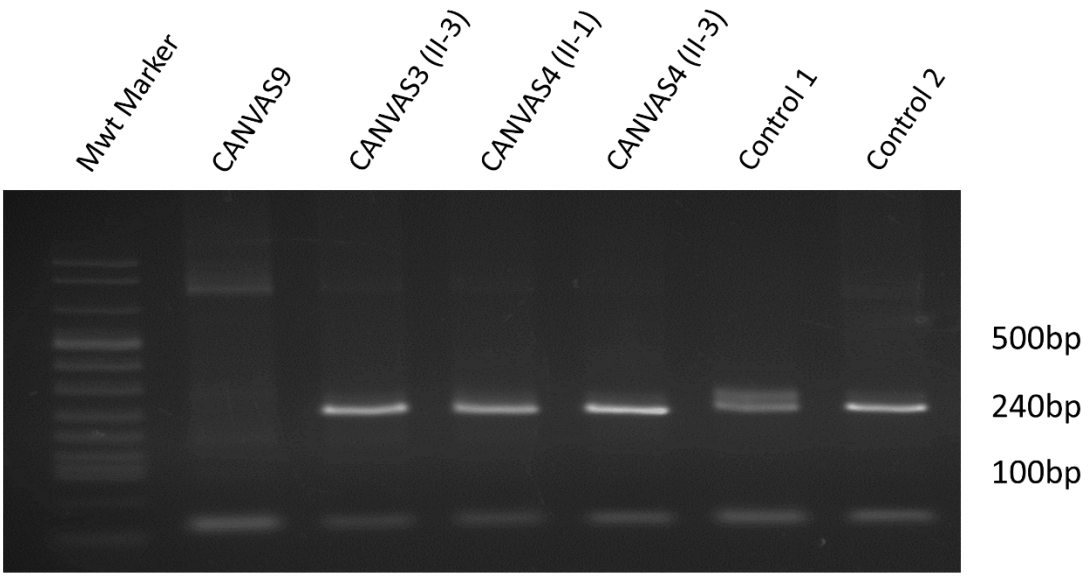

Figure S5: PCR analysis of unaffected individuals from *RFC1* linked CANVAS families. Genomic DNA from three unaffected family members from CANVAS3 and CANVAS4 was analysed for the presence of a non-expanded *RFC1* allele. All three individuals carried at least one non-expanded allele, as indicated by the ~250bp PCR product. CANVAS9 is homozygous for the expanded allele and indicates the pattern expected in the absence of the reference allele. Pedigree structure and affected status are illustrated in Figure S1.

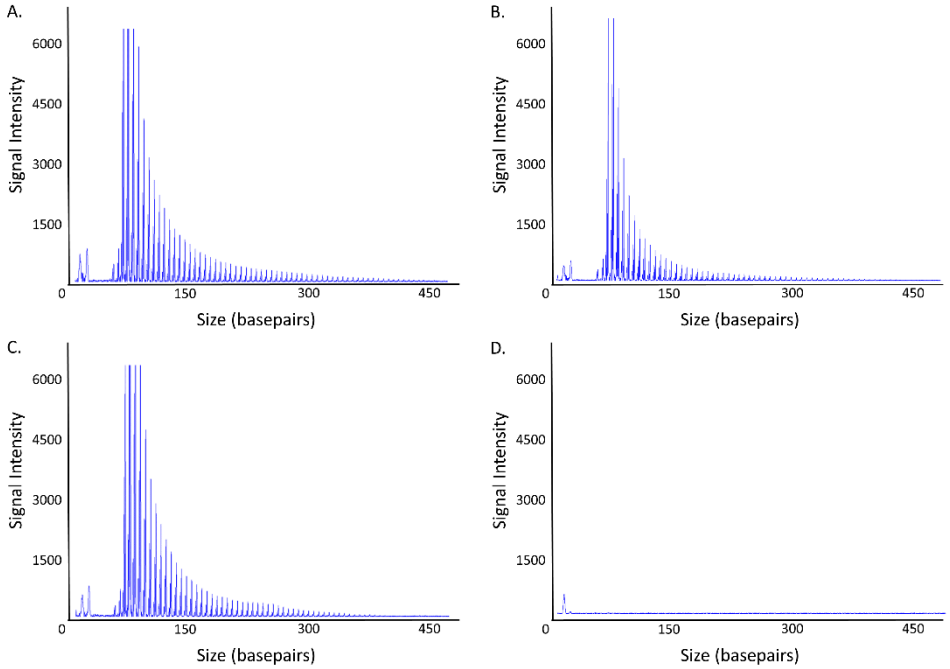

Figure S6: Repeat-primed PCR analysis of unaffected individuals with (AAGGG)exp RE. Representative images of the repeat-primed PCR for the (AAGGG)exp RE demonstrating a saw-toothed product with 5 base pair repeat unit size, amplified from gDNA of control individuals with heterozygous (A, B) or homozygous (C) alleles encoding the (AAGGG)exp RE. No product was observed for the no gDNA template negative control (D).

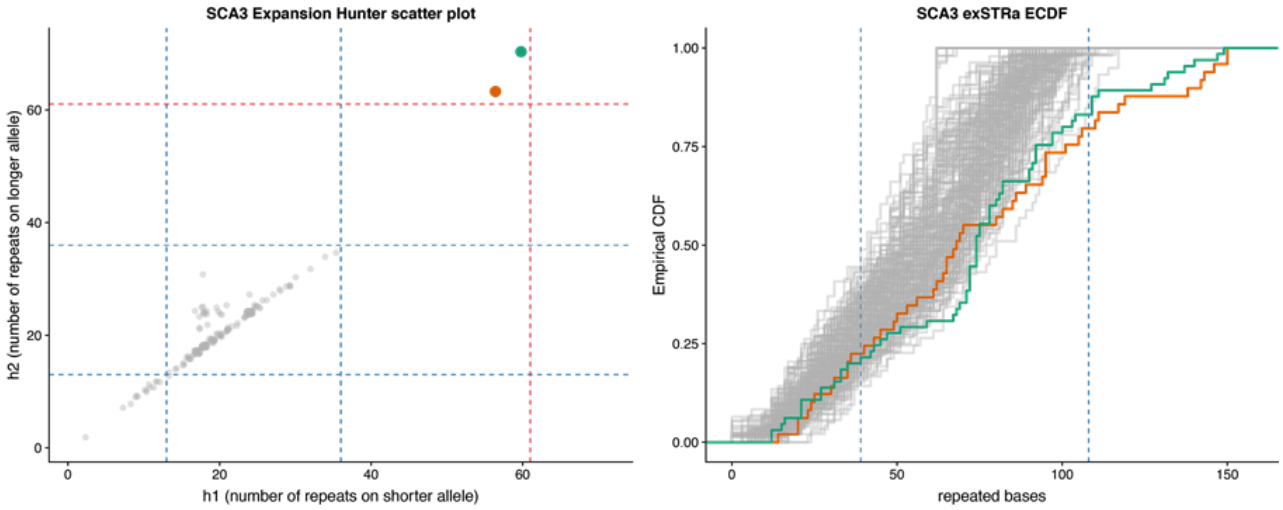

Figure S7: Identification of a pathogenic SCA3 expansion in CANVAS13.

The WGS data for SCA3 (green dot) and an individual with a confirmed SCA3 RE (orange dot) was analysed using ExpansionHunter and exSTRa. This analysis identified a heterozygous, pathogenic SCA3 expansion in CANVAS13.

Primer name	Position (hg19)	Sequence
CANVAS_RFC1_3F	chr4: 39350172-39350192	5'-ACTGACAGTGTTTTTGCCTGT
CANVAS_RFC1_3R	chr4:39349940-39349959	5'-GGCTGAGGCAGGAGATTCAC
TPP_CANVAS_FAM_2F	chr4:39350172-39350192	FAM-5'-ACTGACAGTGTTTTTGCCTGT
5R_TPP_M13R_CANVAS_RE_R	NA	5'-CAGGAAACAGCTATGACC_AAGGGAAGGGAAGGGAAGGGAAGGG
TPP_M13R	NA	5'-CAGGAAACAGCTATGACC

Table S1: Primer sequences for analysis of RFC1.

The gene reference sequences utilized were NC_000004.11 and NM_002913.4 (*RFC1*).

ENSEMBL Gene ID	Gene name	Gene biotype	OMIM gene ID	OMIM disease phenotype (phenotype, OMIM phenotype ID, inheritance pattern)
ENSG00000121895	TMEM156	protein_coding	NA	NA
ENSG00000109790	KLHL5	protein_coding	608064	NA
ENSG00000249207	RP11-360F5.1	antisense	NA	NA
ENSG00000249685	RP11-360F5.3	lincRNA	NA	NA
ENSG00000157796	WDR19	protein_coding	608151	?Cranioectodermal dysplasia 4, 614378, AR; ?Short-rib thoracic dysplasia 5 with or without polydactyly, 614376, AR;Nephronophthisis 13, 614377, AR; Senior-Loken syndrome 8, 616307, AR
ENSG00000035928	RFC1	protein_coding	102579	NA
ENSG00000206675	RNU6-32P	snRNA	NA	NA
ENSG00000222592	RNU6-887P	snRNA	NA	NA
ENSG00000134962	KLB	protein_coding	611135	NA
ENSG00000264621	MIR5591	miRNA	NA	NA
ENSG00000238797	Y_RNA	misc_RNA	NA	NA
ENSG00000163682	RPL9	protein_coding	603686	NA
ENSG00000121897	LIAS	protein_coding	607031	Hyperglycinemia, lactic acidosis, and seizures, 614462, AR
ENSG00000224097	RP11-472B18.1	pseudogene	NA	NA
ENSG00000109814	UGDH	protein_coding	603370	NA
ENSG00000249348	UGDH-AS1	antisense	NA	NA
ENSG00000163683	SMIM14	protein_coding	NA	NA
ENSG00000252796	RNU7-11P	snRNA	NA	NA
ENSG00000255458	RP11-539G18.2	lincRNA	NA	NA
ENSG00000078140	UBE2K	protein_coding	602846	NA
ENSG00000252975	Y_RNA	misc_RNA	NA	NA
ENSG00000249019	RP11-539G18.1	pseudogene	NA	NA
ENSG00000243260	RN7SL558P	misc_RNA	NA	NA
ENSG00000180610	ZBTB12P1	pseudogene	NA	NA

ENSG00000121892	PDS5A	protein_coding	613200	NA
ENSG00000271278	TCEB1P33	pseudogene	NA	NA
ENSG00000252970	RNA5SP159	rRNA	NA	NA
ENSG00000250568	RP11-333E13.2	pseudogene	NA	NA
ENSG00000231707	PABPC1P1	pseudogene	NA	NA
ENSG00000249064	KRT18P25	pseudogene	NA	NA
ENSG00000205794	RP11-333E13.4	pseudogene	NA	NA
ENSG00000078177	N4BP2	protein_coding	NA	NA
ENSG00000200455	RNU6-1112P	snRNA	NA	NA
ENSG00000201863	SNORA51	snoRNA	NA	NA
ENSG00000248977	RP11-395I6.1	pseudogene	NA	NA
ENSG00000260296	RP11-395I6.3	sense_overlapping	NA	NA
ENSG00000168421	RHOH	protein_coding	602037	{?Epidermodysplasia verruciformis, susceptibility to, 4}, 618307, AR
ENSG00000250338	RP11-395I6.2	lincRNA	NA	NA
ENSG00000249241	AC195454.1	lincRNA	NA	NA
ENSG00000174343	CHRNA9	protein_coding	605116	NA
ENSG00000239010	RNU7-74P	snRNA	NA	NA
ENSG00000250893	RP11-588L15.2	antisense	NA	NA

Table S2. Genes and known disease associations within the CANVAS linkage region

region	repeat.	pval	adj	Func.refGene	Gene.refGene
chr4:39350095-39350508	AAGGG	0.0027	1	intronic	RFC1
chr5:68499727-68500146	AATATATATATATAG	0.0027	1	intronic	CENPH
chr7:157344383-157344946	ACAGCCACCACCCACCCC	0.0027	1	intronic	PTPRN2
chr9:138739792-138740277	AAGGGGAGGGGAGTGGGGGG	0.0027	1	intronic	CAMSAP1
chr11:100495523-100496852	AATATGTGTATATATGT	0.0027	1	intergenic	CNTN5; LOC100128386
chr11:127149089-127150146	AAG	0.0027	1	ncRNA_intronic	LOC101929497
chr19:43901669-43901885	AAATATATATTATATAT	0.0027	1	intronic	TEX101
chr20:43066951-43067388	AAAAATATAATATAT	0.0027	1	intergenic	HNF4A; LINC01430
chr3:175416044-175416658	ACACATACATATAT	0.0028	1	intronic	NAALADL2
chr5:4286195-4286524	AAGCTATATATATATAGTG	0.0028	1	intergenic	IRX1; LINC02114
chr5:74613999-74614513	AAAG	0.0028	1	intergenic	ANKRD31; HMGCR
chr6:165352545-165353525	AAAG	0.0028	1	intergenic	MEAT6; C6orf118
chr7:4930864-4931703	AGAT	0.0028	1	intergenic	RADIL; MMD2
chr7:157846063-157847123	ACCCCAGAGACGCAGAG	0.0028	1	intronic	PTPRN2
chr10:134789654-134790481	AATACATTCCACGTGTATC	0.0028	1	ncRNA_exonic	LINC01168
chr11:2182294-2182840	ACACCCCTGTCCCC	0.0028	1	UTR5	INS; INS-IGF2
chr11:120746805-120747444	ACC	0.0028	1	ncRNA_intronic	LOC101929227
chr11:134177695-134179032	ACC	0.0028	1	intronic	GLB1L3
chr13:40788773-40788913	AATATAT	0.0028	1	ncRNA_intronic	LINC00548

Table S3: Expansion Hunter de novo results - screening for RE in two CANVAS individuals compared to 31 controls (all PCR based WGS, p < 0.01) ranked by p-value and ordered by chromosome

position	REF	ALT	genes	region	SNP	MAF	CANVAS1	CANVAS2	CANVAS3	CANVAS4	CANVAS6	CANVAS7	CANVAS8	CANVAS9	CANVAS10	CANVAS12	CANVAS18	CANVAS14	Core haplotype
38777173	A	T	TLR10	exonic	rs10856838	0.2806	0/0		0/0	0/1	0/1	1/1	0/0	0/0	0/0	0/1	0/1	0/0	
38777236	T	G	TLR10	UTR5	rs10856839	0.2803	0/0	0/0	0/0	0/1	0/1	1/1	0/0	0/0	0/0	0/1	0/1	0/0	
38798515	G	A	TLR1	exonic	rs72493538	0.0063	0/0	0/0	0/0	0/0	0/0	0/1	0/0	0/0	0/0	0/0	0/0	0/0	
38798648	C	A	TLR1	exonic	rs5743618	0.4732	0/0	0/1	0/0	1/1	0/0	1/1	0/0	1/1	0/0	1/1	1/1	1/1	
38798935	C	T	TLR1	exonic	rs5743614	0.3942	0/0	0/1	0/0	1/1	0/0	0/1	0/0	0/0	0/0	1/1	0/1	1/1	
38799269	G	A	TLR1	exonic	rs770320905	3.23E-05	0/0	0/0	0/0	0/1	0/0	0/0	0/0	0/0	0/0	0/0	0/0	0/0	
38799539	T	A	TLR1	exonic	rs3923647	0.0364	0/0	0/0	0/0	0/0	0/0	0/0	0/0	0/0	0/0	0/0	0/0	1/1	
38799710	T	C	TLR1	exonic	rs4833095	0.4041	0/0	0/1	0/0	1/1	0/0	0/1	0/0	0/0	0/0	1/1	0/1	1/1	
38800214	C	G	TLR1	exonic	rs5743611	0.1029	0/0	0/0	0/0	0/0	0/1	0/0	0/0	0/0	0/0	0/0	0/0	0/0	
38829163	A	C	TLR6	exonic	rs5743818	0.2286	1/1	0/0	0/1	0/0	0/1	0/0	0/0	0/0	0/0	0/0	0/0	0/0	
38829832	T	C	TLR6	exonic	rs3775073	0.4618	1/1	0/0	0/1	0/1	0/1	0/0	0/0	0/0	0/0	0/1	0/1	1/1	
38830012	G	C	TLR6	exonic	rs3821985	0.4546	1/1	0/0	0/1	0/1	0/1	0/0	0/0	0/0	0/0	0/1	0/1	1/1	
38830116	C	T	TLR6	exonic	rs3796508	0.0134	0/0	0/0	0/0	0/1	0/0	0/0	0/0	0/0	0/0	0/1	0/1	0/0	
38830350	A	G	TLR6	exonic	rs5743810	0.7116	1/1	0/1	1/1	1/1	0/1	1/1	0/0	0/0	0/0	1/1	1/1	1/1	
38830736	A	G	TLR6	exonic	rs5743808	0.0336	0/0	0/0	0/0	0/1	0/0	0/0	0/0	0/0	0/0	0/1	0/1	0/0	
38879655	C	T	FAM114A1	intronic	rs73236661	0.3071	1/1	0/0	0/1	0/1	0/1	0/0	0/0	0/0	0/0	0/0	0/1	0/0	
38879949	G	A	FAM114A1	exonic	rs11096964	0.308	1/1	0/0	0/1	0/1	0/1	0/0	0/0	0/0	0/0	0/0	0/1	0/0	
38880046	T	C	FAM114A1	exonic	rs11555334	0.3075	1/1	0/0	0/1	0/1	0/1	0/0	0/0	0/0	0/0	0/0	0/1	0/0	
38880136	A	T	FAM114A1	intronic	rs11943209	0.308	1/1	0/0	0/1	0/1	0/1	0/0	0/0	0/0	0/0	0/0	0/1	0/0	
38880167	C	T	FAM114A1	intronic	rs11938589	0.308	1/1	0/0	0/1	0/1	0/1	0/0	0/0	0/0	0/0	0/0	0/1	0/0	
38880181	A	ATGTGT	FAM114A1	intronic	rs111676993	0.3053	1/1	0/0	0/1	0/1	0/1	0/0	0/0	0/0	0/0	0/0	0/1	0/0	
38924358	A	G	FAM114A1	intronic	rs12498685	0.1954	1/1	0/0	0/1	0/0	0/0	1/1	0/0	0/0	0/0	0/0	0/0	0/0	
38930921	A	G	FAM114A1	exonic	rs3188469	0.1131	1/1	0/0	0/1	0/0	0/0	0/0	0/0	0/0	0/0	0/0	0/0	0/0	
38930985	T	TAA	FAM114A1	intronic	rs35369040	0.2194	0/0	0/0	0/1	0/1	0/0	0/0	0/0	1/1	0/0	0/0	0/0	0/0	
38930995	C	A	FAM114A1	intronic	rs58035134	0.2307	0/0	0/0	0/1	0/1	0/0	0/0	0/0	1/1	0/0	0/0	0/0	0/0	
38937372	T	C	FAM114A1	exonic	rs2271031	0.6742	1/1	0/0	1/1	1/1	1/1	1/1	0/1	1/1	0/0	0/0	0/0	0/0	
38944976	A	AT	FAM114A1	intronic	rs34903665	0.6885	1/1	0/1	0/1	0/1	1/1	0/0	0/1	1/1	0/0	0/1	0/1	0/0	
38945169	A	G	FAM114A1	exonic	rs1060582	0.1114	0/1	0/0	0/0	0/0	0/0	0/0	0/0	0/0	0/0	0/0	0/0	0/0	
38972691	T	C	TMEM156	exonic	rs140693293	0.0038	0/0	0/0	0/0	0/0	0/0	0/0	0/0	0/0	0/0	0/1	0/0	0/0	
38972793	A	G	TMEM156	intronic	rs3733268	0.0197	0/0	0/1	0/0	0/0	0/0	0/0	0/0	0/0	0/0	0/0	0/0	0/0	
38990334	C	T	TMEM156	intronic	rs3821986	0.4426	0/1	1/1	1/1	0/1	1/1	0/0	1/1	0/0	0/1	1/1	1/1	0/0	
38995310	A	G	TMEM156	intronic	rs11721954	0.3605	0/0	0/0	0/1	0/0	0/0	0/0	0/1	0/0	0/1	1/1	1/1	0/0	
38995374	T	C	TMEM156	exonic	rs10212770	0.88	0/1	1/1	1/1	1/1	1/1	1/1	1/1	1/1	1/1	1/1	1/1	0/0	C
39000305	A	G	TMEM156	exonic	rs11542133	0.23	0/0	0/0	0/0	0/0	0/0	0/0	0/0	0/0	0/1	0/1	0/0	0/0	A
39064126	G	C	KLHL5	UTR5	rs2711942	0.74	0/1	1/1	1/1	1/1	1/1	0/0	0/0	1/1	1/1	1/1	1/1	1/1	C
39064162	A	C	KLHL5	exonic	rs2711941	0.74	0/1	1/1	1/1	1/1	1/1	0/0	0/0	1/1	1/1	1/1	1/1	1/1	C
39077567	G	GT	KLHL5	intronic	rs201873328	0.02	0/0	0/0	0/0	0/0	0/0	0/0	0/0	0/0	0/1	0/0	0/0	0/0	G
39114929	G	A	KLHL5	intronic	rs3796510	0.53	0/0	0/0	0/0	0/0	0/0	0/0	0/1	0/0	0/0	0/0	0/0	1/1	G
39116775	A	T	KLHL5	intronic	rs10026775	0.53	0/0	0/0	0/0	0/0	0/0	0/0	0/1	0/0	0/0	0/0	0/0	1/1	A
39116911	T	C	KLHL5	exonic	rs3733276	0.53	0/0	0/0	0/0	0/0	0/0	0/0	0/1	0/0	0/0	0/0	0/0	1/1	T
39117103	G	A	KLHL5	intronic	rs3733277	0.53	0/0	0/0	0/0	0/0	0/0	0/0	0/1	0/0	0/0	0/0	0/0	1/1	G
39205365	C	T	WDR19	intronic	rs1451817	0.97	1/1	1/1	1/1	1/1	1/1	1/1	1/1	1/1	1/1	1/1	1/1	1/1	T
39216221	C	T	WDR19	exonic	rs2167494	0.29	0/1	0/0	0/0	0/0	0/0	0/0	0/1	0/0	0/0	0/0	0/0	0/0	C
39216240	G	A	WDR19	exonic	rs75964850	0.04	0/0	0/0	0/0	0/0	0/0	0/0	0/1	0/0	0/0	0/0	0/0	0/0	G
39217779	C	T	WDR19	exonic	rs199765304	0	0/0	0/0	0/0	0/0	0/0	0/0	0/1	0/0	0/0	0/0	0/0	0/0	A
39229771	G	A	WDR19	intronic	rs11730558	0.31	0/1	0/0	0/0	0/0	0/0	0/0	0/1	0/0	0/0	0/0	0/0	0/0	G
39242111	C	A	WDR19	intronic	rs9998591	0.64	0/1	1/1	1/1	1/1	1/1	1/1	0/1	1/1	1/1	1/1	1/1	1/1	A
39254828	A	C	WDR19	exonic	rs187546086	0	0/1	0/0	0/0	0/0	0/0	0/0	0/0	0/0	0/0	0/0	0/0	0/0	A
39255496	A	G	WDR19	intronic	rs33997556	0.08	0/1	1/1	1/1	1/1	1/1	1/1	0/1	1/1	1/1	1/1	1/1	0/0	G
39271541	A	G	WDR19	intronic	rs3733280	0.31	0/1	0/0	0/0	0/0	0/0	0/0	0/1	0/0	0/0	0/0	1/1	0/0	A
39276623	A	AG	WDR19	intronic	rs11096989	0.5	1/1	1/1	1/1	1/1	1/1	1/1	1/1	1/1	1/1	1/1	1/1	0/0	AG
39279724	T	C	WDR19	intronic	rs12648082	0.5	1/1	1/1	1/1	1/1	1/1	1/1	1/1	1/1	1/1	1/1	1/1	0/0	C
39279907	A	G	WDR19	intronic	rs2276888	0.46	0/0	0/0	0/0	0/0	0/0	0/0	0/0	0/0	0/0	0/0	0/0	1/1	A
39297211	C	T	RFC1	intronic	rs41547922	0	0/0	0/0	0/1	0/1	0/0	0/0	0/0	0/0	0/0	0/0	0/0	0/0	C
39301605	G	C	RFC1	intronic	rs2066788	0.51	1/1	1/1	1/1	1/1	1/1	1/1	1/1	1/1	1/1	1/1	1/1	0/0	C
39302029	T	C	RFC1	exonic	rs2066786	0.45	0/0	0/0	0/0	0/0	0/0	0/0	0/0	0/0	0/0	0/0	0/0	1/1	T
39303925	A	G	RFC1	exonic	rs2066782	0.1	1/1	1/1	1/1	1/1	1/1	1/1	0/1	1/1	1/1	1/1	0/0	0/0	G
39329102	G	A	RFC1	intronic	rs11096992	0.47	1/1	1/1	1/1	1/1	1/1	1/1	1/1	1/1	1/1	1/1	1/1	1/1	A
39353122	C	T	RFC1	intronic	rs4975007	0.98	1/1	1/1	1/1	1/1	1/1	1/1	1/1	1/1	1/1	1/1	1/1	1/1	T
39353137	C	T	RFC1	intronic	rs374311239	0	0/0	0/1	0/0	0/0	0/0	0/0	0/0	0/0	0/0	0/0	0/0	0/0	C
39439264	T	C	KLB	intronic	rs4975015	0.1707	0/1	0/0	0/1	0/0	0/0	0/0	1/1	1/1	1/1	0/0	0/0	1/1	C
39448529	G	A	KLB	exonic	rs17618244	0.1528	0/0	0/1	0/0	0/0	1/1	0/0	0/0	0/0	0/0	0/1	1/1	0/0	G
39448542	C	G	KLB	exonic	rs7685429	0.7326	1/1	1/1	0/1	1/1	1/1	1/1	0/0	1/1	1/1	0/1	1/1	0/0	G
39448586	C	T	KLB	exonic	rs35372803	0.0375	0/0	0/1	0/0	0/0	0/0	0/0	0/0	0/0	0/0	0/0	0/0	0/0	C
39450229	C	A	KLB	exonic	rs4975017	0.2881	0/1	0/0	0/0	0/0	0/0	0/0	0/0	0/0	1/1	0/0	0/0	0/0	
39450403	TGA	T	KLB	UTR3	rs112327399	0.0603	0/0	0/0	0/0	0/0	0/0	0/0	0/0	1/1	0/0	0/0	0/0	0/0	
39457857	T	C	RPL9	intronic	rs1015450	0.1489	0/1	0/1	0/0	0/1	0/0	0/0	0/0	0/0	0/0	0/0	0/0	0/0	
39457870	T	TG	RPL9	intronic	rs3216720	0.6465	1/1	1/1	0/1	1/1	1/1	1/1	0/0	0/0	1/1	0/1	1/1	0/0	
39457954	G	C	RPL9	intronic	rs117602443	6.00E-04	0/0	0/0	0/0	0/0	0/0	0/0	0/0	0/0	0/0	0/1	0/0	0/0	
39459724	T	C	RPL9	intronic	rs2687958	0.6479	1/1	1/1	0/1	1/1	1/1	1/1	0/0	0/0	1/1	0/1	1/1	0/0	
39460328	G	A	RPL9	intronic	rs73137448	0.0563	0/0	0/0	0/0	0/0	0/0	0/0	0/0	1/1	0/0	0/0	0/0	0/0	
39460352	C	G	RPL9	intronic	rs11550000	0.2497	0/1	0/1	0/0	0/1	0/0	0/0	0/0	1/1	0/0	0/0	0/0	0/0	
39460413	C	A	RPL9	intronic	rs2276889	0.0234	0/0	0/0	0/1	0/1	0/0	1/1	0/0	0/0	0/0	0/0	0/0	0/0	
39460490	C	G	RPL9	intronic	rs2276890	0.2844	0/1	0/0	0/0	0/0	0/0	0/0	0/0	0/0	1/1	0/0	0/0	0/0	
39460539	G	A	RPL9	UTR5	rs116433592	0.005	0/1	0/0	0/0	0/0	0/0	0/0	0/0	0/0	0/0	0/0	0/0	0/0	
39460572	G	A	LIAS\x3bRPL9	upstream	rs3821989	0.006	0/0	0/0	0/0	0/0	0/0	0/0	0/0	0/0	0/0	0/1	0/0	0/0	
39460797	G	A	LIAS	intronic	rs2687959	0.1826	0/0	0/1	0/1	0/1	1/1	1/1	0/0	0/0	0/0	0/1	1/1	0/0	
39466639	A	G	LIAS	intronic	rs76534325	0.0378	0/0	0/0	0/0	0/0	0/0	0/0	0/0	1/1	0/0	0/0	0/0	0/0	
39469279	A	T	LIAS	intronic	rs79572060	0.0233	0/0	0/0	0/1	0/1	0/0	1/1	0/0	0/0	0/0	0/0	0/0	0/0	
39472786	C	T	LIAS	intronic	rs79140300	0.0308	0/0	0/0	0/1	0/1	0/0	1/1	0/0	0/0	0/0	0/0	0/0	0/0	
39472796	T	A	LIAS	intronic	rs73137454	0.0747	0/0	0/0	0/0	0/0	0/0	0/0	0/0	1/1	0/0	0/0	0/0	0/0	
39472842	T	A	LIAS	intronic	rs2125314	0.3142	0/1	0/0	0/0	0/0	0/0	0/0	0/0	0/0	1/1	0/0	0/0	0/0	
39474868	G	A	LIAS	intronic	rs749915	0.236	0/1	0/1	0/0	0/1	0/0	0/0	0/0	1/1	0/0	0/0	0/0	0/0	
39482384	A	G	LOC401127	ncRNA exonic	rs10009841	0.0747	0/0	0/0	0/0	0/0	0/0	0/0	0/0	1/1	0/0	0/0	0/0	0/0	
39482440	G	A	LOC401127	ncRNA exonic	rs2276891	0.0232	0/0	0/0	0/1	0/1	0/0	1/1	0/0	0/0	0/0	0/0	0/0	0/0	
39482584	T	C	LOC401127	ncRNA exonic	rs17438520	0.0259	0/1	0/0	0/0	0/0	0/0	0/0	0/0	0/0	1/1	0/0	0/0	0/0	
39482627	T	C	LOC401127	ncRNA exonic	rs2276893	0.0232	0/0	0/0	0/1	0/1	0/0	1/1	0/0	0/0	0/0	0/0	0/0	0/0	
39483115	A	G	LOC401127	ncRNA exonic	rs2687980	0.7109	1/1	1/1	0/1	1/1	1/1	1/1	0/0	1/1	1/1	0/1	1/1	0/0	
39506144	C	T	UGDH	intronic	rs1379819	0.1465	0/0	0/0	0/0	0/0	0/0	0/0	0/0	0/0	0/0	1/1	0/0	0/0	
39506997	GA	G	UGDH	intronic	rs33942301	0.248	0/1	0/0	0/1	0/1	0/0	1/1	0/0	0/0	1/1	1/1	0/0	0/0	
39507083	G	T	UGDH	intronic	rs4975019	0.3746	0/1	0/0	0/1	1/1	0/0	1/1	0/0	0/0	1/1	1/1	0/0	0/0	
39510175	G	A	UGDH	intronic	rs6815780	0.2211	0/1	0/0	0/1	0/1	0/0	1/1	0/0	0/0	1/1	1/1	0/0	0/0	
39510264	A	G	UGDH	exonic	rs1129052	0.2203	0/1	0/0	0/1	0/1	0/0	1/1	0/0	0/0	1/1	1/1	0/0	0/0	
39511359	T	C	UGDH	intronic	rs6531722	0.2211	0/1	0/0	0/1	0/1	0/0	1/1	0/0	0/0	1/1	1/1	0/0	0/0	
39512347	T	C	UGDH	exonic	rs11544855	0.1145	0/0	0/0	0/1	0/0	0/0	0/0	1/1	0/0	0/0	0/0	0/0	1/1	
39515736	A	G	UGDH	exonic	rs10019532	0.213	0/1	0/0	0/1	0/1	0/0	1/1	0/0	0/0	1/1	1/1	0/0	0/0	
39515806	TAAAAAGA	T	UGDH	intronic	rs151116497	0.1451	0/0	0/0	0/0	0/0	0/0	0/0	0/0	0/0	0/0	1/1	0/0	0/0	
39528752	G	A	UGDH	intronic	rs4975020	0.7065	1/1	0/1	1/1	1/1	0/0	1/1	1/1	0/0	1/1	1/1	1/1	1/1	
39606900	T	C	SMIM14	intronic	rs147611359	0.0076	0/0	0/0	0/0	0/0	0/0	0/0	0/1	0/0	0/0	0/0	0/0	0/0	
39757480	A	AT	UBE2K	intronic	rs11389468	0.8191	1/1	1/1	0/1	1/1	0/0	1/1	0/1	1/1	0/1	1/1	1/1	1/1	
39757525	C	T	UBE2K	intronic	rs138858087	0.0072	0/0	0/0	0/0	0/0	0/0	0/0	0/1	0/0	0/0	0/0	0/0	0/0	
39871117	G	GA	PDSSA	intronic	rs34039605	0.3225	0/1	1/1	0/0	0/1	0/0	0/0	0/0	1/1	0/1	1/1	1/1	0/0	
39900041	T	C	PDSSA	exonic	rs193075238	3.24E-05	0/0	0/0	0/0	0/0	0/0	0/0	0/0	0/0	0/0	0/0	1/1	0/0	
39903924	G	A	PDSSA	intronic	rs77174235	0.0728	0/1	0/1	0/0	0/1	0/0	0/0	0/0	1/1	0/1	0/0	0/0	0/0	

Table S4. CANVAS core haplotype from WES data (core haplotype shown in dark green)